



Published in final edited form as:

Biochemistry. 2010 May 25; 49(20): 4361–4373. doi:10.1021/bi100092a.

## Probing DNA Binding, DNA Opening and Assembly of a Downstream Clamp/Jaw in *E. coli* RNA Polymerase – $\lambda P_R$ Promoter Complexes Using Salt and the Physiological Anion Glutamate<sup>†</sup>

Wayne S. Kontur<sup>‡,¶,1</sup>, Michael W. Capp<sup>§,¶</sup>, Theodore J. Gries<sup>§</sup>, Ruth M. Saecker<sup>§,\*</sup>, and M. Thomas Record Jr.<sup>‡,§,\*</sup>

<sup>‡</sup>Department of Chemistry University of Wisconsin-Madison, Madison WI 53706

<sup>§</sup>Department of Biochemistry University of Wisconsin-Madison, Madison WI 53706

### Abstract

Transcription by all RNA polymerases (RNAP) requires a series of large-scale conformational changes to form the transcriptionally-competent open complex  $RP_o$ . At the  $\lambda P_R$  promoter, *E. coli*  $\sigma^{70}$  RNAP first forms a wrapped, closed 100 bp complex  $I_1$ . The subsequent step opens the entire 13 base DNA bubble, creating the relatively unstable (open) complex  $I_2$ . Additional conformational changes convert  $I_2$  to the stable  $RP_o$ . Here we probe these events by dissecting the effects of  $Na^+$  salts of  $Glu^-$ ,  $F^-$  and  $Cl^-$  on each step in this critical process. Rapid mixing and nitrocellulose filter binding reveal that the binding constant for  $I_1$  at 25 °C is ~30-fold larger in  $Glu^-$  than in  $Cl^-$  at the same  $[Na^+]$ , with the same log-log [salt] dependence for both anions. In contrast, both the rate constant and equilibrium constant for DNA opening ( $I_1$  to  $I_2$ ) are only weakly [salt]-dependent, and the opening rate constant is insensitive to replacement of  $Cl^-$  by  $Glu^-$ . These very small effects of [salt] on a process (DNA opening) which is strongly [salt]-dependent in solution may indicate that the backbones of both DNA strands interact with polymerase throughout the process, and/or that compensation is present between ion uptake and release.

Replacement of  $Cl^-$  by  $Glu^-$  or  $F^-$  at 25 °C greatly increases the lifetime of  $RP_o$  and greatly reduces its [salt]-dependence. By analogy to Hofmeister salt effects on protein folding, we propose that the excluded anions  $Glu^-$  and  $F^-$  drive the folding and assembly of the RNAP clamp/jaw domains in the conversion of  $I_2$  to  $RP_o$ , while  $Cl^-$  does not. Because the Hofmeister effect of these anions largely compensates for the destabilizing coulombic effect of any salt on the binding of this assembly to downstream promoter DNA,  $RP_o$  remains long-lived even at 0.5 M  $Na^+$  in  $Glu^-$  or  $F^-$  salts. The observation that  $E\sigma^{70} RP_o$  are exceedingly long-lived in moderate to high  $[Glu^-]$  argues that  $E\sigma^{70}$  RNAP do not dissociate from strong promoters *in vivo* when the cytoplasmic increases during osmotic stress.

<sup>†</sup>This work was supported by NIH grant GM23467 to M.T. R. W. S. K. gratefully acknowledges the support of the Biotechnology Training Program (NIH 5 T32 GM08349); T. G. is the recipient of the William R. and Dorothy E. Sullivan Distinguished Graduate Fellowship.

\*To whom correspondence should be addressed: Telephone 608-262-5332, FAX 608-262-3453 mtrecord@wisc.edu, rmsaecker@wisc.edu.

<sup>¶</sup>These authors contributed equally to this work.

<sup>1</sup>Current address: Department of Bacteriology, University of Wisconsin-Madison/Great Lakes Bioenergy Research Center, Madison, WI 53706

### Supporting Information

Supporting information reports the irreversible rate constants ( $k_{obs}$ ) for formation of open complexes as a function of  $[RNAP]_{total}$  and  $[Na^+]$  in  $Cl^-$  buffer (STable 1), and in  $Glu^-$  and  $F^-$  buffers (STable 2). STable 3 presents the fits ( $K_{heparin}$ ,  $[R]_{free}$ ) of relaxation to equilibrium data ( $k_r$ ) at 25 °C to obtain  $k_d$  in  $Glu^-$  and  $F^-$  buffers. This material is available free of charge via the Internet at <http://pubs.acs.org>.

*E. coli* cells have the remarkable ability to grow over a very wide range of environmental conditions, including osmotic conditions ranging from very dilute (0.02 osmolal) to concentrated, high [salt] media (> 3 osmolal) (3-5). In vivo, increases in external osmolarity, which increase cytoplasmic [K<sup>+</sup>] and [Glu<sup>-</sup>], reduce bulk transcription (6) while transcription from genes involved in the osmotic stress response selectively increases (7-9). In the absence of any known osmosensing (e.g. glutamate binding) transcription factor, the simplest hypothesis is that changes in cytoplasmic [K<sup>+</sup>] and [Glu<sup>-</sup>] alone alter transcription (10) during the initial response to osmotic upshift. What features of RNA polymerase and promoter sequence allow the cell to achieve a dramatic reprogramming to maintain homeostasis?

Understanding how cells regulate their gene expression requires kinetic-mechanistic studies. Although transcription by *E. coli* RNAP has been studied in vivo and in vitro for four decades, we are only beginning to understand the workings of this machine at a molecular level. Key questions are how is DNA opened by RNAP and what significant conformational changes occur during the steps that precede and follow this central DNA opening step? How do variables like the identity of the sigma specificity subunit, the promoter DNA sequence, supercoiling, concentrations of solutes, small ligands, or regulatory proteins affect the rate of formation and lifetime of the transcriptionally-competent open complex, and thereby alter the frequency of productive versus abortive initiation from the promoter?

Because the RNAP machinery and promoter organization are conserved, it likely that the sequence of conformational changes that form the bacterial RP<sub>o</sub> is largely invariant (promoter DNA recognition, DNA opening, stabilization of RP<sub>o</sub>), but that the rates of interconversion and populations of initiation intermediates differ as a function of the variables noted above. Here we investigate how the substitution of the physiological anion Glu<sup>-</sup> for the laboratory anion Cl<sup>-</sup> affects each step in the process of open complex formation at the λP<sub>R</sub> promoter by the housekeeping form of *E. coli* RNA polymerase (RNAP, subunit composition σ<sup>70</sup>α<sub>2</sub>ββ'ω). While our research focuses on this promoter, we expect that these results reflect the salient functional characteristics of many Eσ<sup>70</sup> RNAP promoter interactions.

In vitro, changes in salt concentration profoundly affect both the composite second order association rate constant (k<sub>a</sub>) and composite dissociation rate constant (k<sub>d</sub>) for the formation and dissociation of RP<sub>o</sub> at the σP<sub>R</sub> promoter, respectively (11,12). One contributor to these salt effects is coulombic: positively charged residues in the promoter-RNAP interface reduce the high negative phosphate charge density of DNA, releasing locally accumulated salt ions (e.g. K<sup>+</sup> or Na<sup>+</sup> from DNA). In addition, the identity of the anion has large effects on the magnitude of k<sub>a</sub>: for the σP<sub>R</sub> promoter k<sub>a</sub> was found to be at least 30-fold larger in glutamate (Glu<sup>-</sup>) than in chloride (Cl<sup>-</sup>) at 0.20 M K<sup>+</sup> (13). Here we dissect this large salt anion effect. Large effects of substituting another anion for Cl<sup>-</sup> are also observed for many other nucleic acid DNA binding proteins, including transcription factors (14-16), helicases (15), T7 RNAP (17) and DNA polymerases. Large Hofmeister effects of salt anions like Glu<sup>-</sup> and F<sup>-</sup>, relative to Cl<sup>-</sup>, are expected on steps in which interface formation or coupled folding buries large amounts of nonpolar (hydrocarbon) surface (18,19).

At the strong λP<sub>R</sub> promoter (P), the mechanism of open complex formation consists of a minimum of three steps, proceeding through two kinetically significant intermediates (11, 20-22)



where R represents RNA polymerase  $E\sigma^{70}$ , P is promoter, and  $I_1$  and  $I_2$  are the first and second kinetically significant intermediates, respectively. Opening of the entire DNA bubble (-11 to +2) occurs in the conversion of  $I_1$  to  $I_2$  ((23); Gries et al., unpublished). No other early intermediates are kinetically significant at the  $\lambda P_R$  promoter. Solute upshift studies designed to study the late steps in  $RP_o$  formation reveal the existence of an intermediate ( $I_3$ ) forming after  $I_2$  and directly preceding the formation of  $RP_o$  (24).  $I_3$  rapidly equilibrates with  $I_2$  and  $RP_o$  under the conditions of this study, and thus can be neglected in the analysis of  $k_d$  presented here. Because the kinetics of open complex formation (association) and dissociation are single exponential for almost all conditions examined, we deduce that: i. in association  $I_1$  rapidly equilibrates with free RNAP and promoter DNA on the time scale required for  $I_1$  to convert to  $I_2$  in the forward direction ( $k_{-1} \gg k_2$ ); and ii.  $I_2$  rapidly equilibrates with  $RP_o$  on the time scale required for  $I_2$  to convert to  $I_1$  in the reverse direction ( $k_3 \gg k_{-2}$ ). The interconversions of  $I_1$  and  $I_2$  are the bottleneck steps in both the association and dissociation directions.

Using rapid mixing we recently dissected the composite association and dissociation rate constants for RNAP-  $\lambda P_R$  interactions into their individual contributions from  $K_1 (=k_1/k_{-1})$ ,  $k_2$ ,  $k_{-2}$  and  $K_3 (=k_3/k_{-3})$ , respectively (22,24). We discovered that destabilizing  $RP_o$  by a rapid upshift in salt or urea concentration creates a transient burst of  $I_2$  (24). Coupling rapid mixing with filter binding, we determined the kinetics of forming this unstable open complex ( $I_2$ ) from the stable open complex  $RP_o$ , and converting  $I_2$  to the closed complex  $I_1$  over a wide range of salt concentrations at 10 °C and 37 °C. These studies dissected the effect of [salt] on the dissociation kinetics for the first time. The rate constant  $k_{-2}$  is independent of salt concentration, while the equilibrium constant for the conversion of  $I_2$  to  $RP_o$  decreases strongly with increasing [salt] (24). Permanganate footprinting of  $I_2$  reveals that all reactive thymines in  $RP_o$  are also reactive in  $I_2$ , demonstrating that the entire transcription bubble is opened in the rate-determining, single step  $I_1 \rightarrow I_2$  (Gries et al., unpublished). Measurements of the time dependence of the decay of permanganate reactivity in conversion of  $I_2$  to  $I_1$  corroborate the rate constant  $k_{-2}$  obtained by rapid mixing and filter binding.

The unexpected result that the rate constant  $k_{-2}$  characterizing the conversion of  $I_2$  to the transition state  $(I_1-I_2)^\ddagger$  is independent of salt concentration motivates the work here to dissect the effects of salt concentration on the steps on the first half of the mechanism, namely the formation of  $I_1$  and the transition between  $I_1$  and  $(I_1-I_2)^\ddagger$ . Melting of DNA in solution is strongly salt concentration dependent (25). How does melting DNA to form the initiation bubble in the isomerization of  $I_1$  to  $I_2$  compare?

To address this question we examine whether the rate constant  $k_2$  characterizing the conversion of  $I_1$  to  $(I_1-I_2)^\ddagger$  is [salt]-dependent. Using rapid mixing and filter binding, we dissect for the first time the overall second order association rate constant  $k_a$  into  $K_1$  and  $k_2$  over a range of NaCl and NaGlu concentrations. In addition, we obtain stringent tests of the single exponential character of both the association kinetic data (in [RNAP] excess) and dissociation kinetic data. These findings demonstrate that the initial steps of association (forming  $I_1$ ) and of dissociation (forming  $I_2$ ) do indeed rapidly equilibrate on the time scale of the subsequent slower conformational change (DNA opening or closing). We use manual mixing filter binding to examine the effects of salt concentration (NaX) and choice of anion ( $X = Cl^-$ ,  $Glu^-$ , or  $F^-$ ) on the dissociation of  $RP_o$  at 25 °C.

We find that each step exhibits a uniquely different dependence on changes in  $[Na^+]$  and choice of anion. While the formation of  $I_1$  and conversion of  $I_2$  to  $RP_o$  exhibit large dependences on both  $[Na^+]$  and anion, the bottleneck DNA opening step ( $I_1 \rightarrow I_2$ ) is relatively insensitive to either solution variable. Formation of  $I_1$  and especially  $RP_o$  are greatly favored in  $Glu^-$  relative to  $Cl^-$ . Together these results shed additional light on the conformational changes occurring in each step, allowing us to refine our current structural-mechanistic hypotheses regarding open

complex formation by *E. coli* RNAP. In particular, we propose that the very large effects of replacing  $\text{Cl}^-$  with  $\text{Glu}^-$  on the steps *after* DNA opening result from burial of hydrocarbon surface of RNAP in coupled folding transitions in late steps (24,26,27).  $\text{Glu}^-$  and  $\text{F}^-$  are more highly excluded from nonpolar surface than is  $\text{Cl}^-$  (18,19). We deduce that these late remodeling events assemble a RNAP clamp/jaw on downstream DNA and contribute significantly to the entropic driving force that stabilizes the open DNA state in  $\text{RP}_o$ .

## MATERIALS AND METHODS

### Buffers

Storage Buffer (SB) for RNA polymerase holoenzyme contained 50% glycerol (v/v), 10 mM Tris-HCl (pH 7.5 at 4 °C), 100 mM NaCl, 0.1 mM dithiothreitol (DTT), and 0.1 mM  $\text{Na}_2\text{EDTA}$ . Binding Buffer for the study of the kinetics of RNAP-promoter binding as a function of univalent salt concentration in the absence of  $\text{Mg}^{2+}$  (BB) contained 10 mM  $\text{Na}_2\text{HPO}_4$  buffer (pH 7.4), 6.5% (v/v) glycerol, 1 mM DTT, 100  $\mu\text{g}/\text{mL}$  BSA, 1.3 mM Tris (pH 7.5 at 4 °C; contributed by the Storage Buffer), and variable  $[\text{NaCl}]$ ,  $[\text{NaGlu}]$  or  $[\text{NaF}]$  to bring  $[\text{Na}^+]$  to the desired value. Wash Buffer (WB) contained 0.1 M NaCl, 10 mM Tris-HCl (pH 8.0 at room temperature), and 0.1 mM  $\text{Na}_2\text{EDTA}$ . Addition of NaGlu did not significantly affect the pH of the Tris-HCl buffer.

### Wild-type $\text{E}\sigma^{70}$ RNA polymerase holoenzyme

*E. coli* K12 wild type RNA polymerase holoenzyme was purified as described in (28) and stored in SB at  $-70$  °C. All [RNAP] reported here are concentrations of active holoenzyme (capable of  $\text{RP}_o$  formation). Activities were determined at the time of use, either by analysis of forward titrations of promoter DNA with RNAP performed in the ‘complete binding of limiting reagent’ regime at 37 °C as described (11) or by comparison of association rate constant for different samples determined at the same total [RNAP]. Typically activities were ~70%. Systematic comparisons of the different preparations showed that no difference in promoter association kinetics between individual tubes or preps, when compared at the same active [RNAP].

### $\lambda\text{P}_R$ promoter DNA

A  $^{32}\text{P}$ -DNA fragment containing the  $\lambda\text{P}_R$  promoter was obtained from the plasmid pBR81 as described in (29). *Bss*H II and *Sma* I cleavage of pBR81 centrally positions the  $\lambda\text{P}_R$  wild-type sequence (−60 to +20) in a fragment which extends from −115 to +76 relative to the transcription start site (+1) of the promoter. The specific activity of the fragment was generally  $\sim 10^8$  cpm/mole.

### Association Kinetics

For conditions where the kinetics are sufficiently slow (e.g. RNAP concentrations below 10 nM at mid-range salt concentrations; high (<0.3M) salt concentrations), manual mixing and filter binding were used to determine the kinetics of formation of long-lived (open) complexes, resistant to a 10 - 30 s heparin challenge. For conditions where the kinetics are too fast (first order rate constant  $k_{\text{obs}} > 0.01 \text{ s}^{-1}$ ) to determine by manual mixing (e.g. low salt and higher RNAP concentrations), rapid mixing (2 ms mixing time; RQF-3, Kintek Corp., Austin TX) followed by filter binding on quenched solutions was used (22). Rapid mixing and manual mixing experiments were performed as described in (22). Concentrations of active RNAP were always in at least 6-fold excess over that of promoter to ensure that the initial bimolecular binding step is pseudo-first order within experimental uncertainty.

## Dissociation Kinetics

### i. Irreversible dissociation initiated by adding heparin to pre-formed $RP_o$ —

Effects of  $[Na^+]$  in  $Cl^-$  buffer on the dissociation of preformed  $\lambda P_R$  DNA (0.08-0.09 nM) and RNAP (10 – 40 nM) open complexes at 25 °C were performed as described in (27).

### ii. Decay to equilibrium assay to determine $k_d$ —

The irreversible dissociation of  $RP_o$  complexes initiated by the addition of excess heparin is exceedingly slow in  $Glu^-$  at 25 °C, yielding poorly determined values of  $k_d$ . Thus to determine  $k_d$  as a function of  $Na^+$  in  $Glu^-$  buffer, we used a decay to equilibrium assay at a low  $[RNAP]$  held constant by an excess of the competitor heparin. In this assay, 7 nM RNAP was initially mixed with a vast excess of heparin (0.1 – 1 mg/mL) at the salt concentration of the experiment. After 60 min of incubation,  $^{32}P$   $\lambda P_R$  DNA (12.5 pM) was added, initiating promoter binding which proceeds to equilibrium at the low  $[RNAP]$  of the experiment. The amount of  $\lambda P_R$  - RNAP open complexes was monitored using nitrocellulose filter binding. Typically  $>10^5$  s was required to approach promoter binding equilibrium. At longer times, a very slow decay of the plateau was noted, probably the result of inactivation of RNAP.

## Nitrocellulose filter binding assays

The amount of open complexes as a function of time and solution condition was determined using nitrocellulose filter binding as described in (22). Studies in  $Glu^-$  and  $F^-$  cannot be performed above 0.70 M  $Na^+$  because filter efficiency becomes too low.

## DATA ANALYSIS

Data were analyzed using either SigmaPlot 6.0 or 2000 (SPSS, Inc. Chicago, IL) on a Dell Optiplex GX270 workstation running Windows XP Professional v. 2002 (Microsoft, Seattle, WA), or using Igor 5.0.3.0 (WaveMetrics, Inc., Lake Oswego, OR) on Dell Inspiron 8100.

### Determination of $k_{obs}$ , $k_a$ , $K_1$ and $k_2$ from the kinetics of formation of open complexes

In excess RNAP, the kinetics of irreversible association of RNAP with  $\lambda P_R$  promoter DNA to form open complexes ( $I_2$ ,  $RP_o$ ) are single exponential (see Results) with observed rate constant  $k_{obs}$ , determined by fitting the fraction of promoter DNA bound in open complexes at time  $t$  ( $\theta_t^{open}$ ) (calculated as described in (22)) versus time to eq 1:

$$\theta_t^{open} = 1 - e^{-k_{obs}t} \quad (1)$$

The rate constant  $k_{obs}$  (previously called  $\alpha_{CR}$ ) is a hyperbolic function of RNAP concentration (22):

$$k_{obs} = \frac{K_1 k_2 [RNAP]}{1 + K_1 [RNAP]} = \frac{k_a [RNAP]}{1 + K_1 [RNAP]} \quad (2)$$

where  $K_1 (= k_1/k_{-1})$  is the equilibrium constant for formation of  $I_1$ ,  $k_2$  is the microscopic rate constant for the subsequent (rate-determining) conversion of  $I_1$  to  $I_2$  in Mechanism I, and  $k_a = K_1 k_2$  is the composite overall second-order association rate constant. The data for  $k_{obs}$  as a function of  $[RNAP]$  in Figs 3 and 4 were weighted by  $1/\sigma^2$ , where  $\sigma$  is the standard deviation of  $k_{obs}$ , and fit to eq 2 to determine values of  $k_a$ ,  $K_1$  and  $k_2$  at each salt concentration investigated.  $K_1 (= k_1/k_{-1})$  is the equilibrium constant for formation of the first kinetically-significant intermediate ( $I_1$ , in rapid equilibrium with free RNAP and DNA),  $k_2 (= k_1)$  is the microscopic rate constant for the subsequent (rate-determining;  $k_2 < k_{-1}$ ) conversion of  $I_1$  to

$I_2$  in Mechanism I, and  $k_a (= K_1 k_2)$  is the composite overall second-order association rate constant. Values of  $k_{obs}$  (weighted by  $1/\sigma^2$ , where  $\sigma$  is the standard deviation of  $k_{obs}$ ) were plotted versus  $[RNAP]$  and fit to eq 2 to determine  $k_a$ ,  $K_1$  and  $k_2$ .

Above 0.23 M  $Na^+$  in NaCl buffer and 0.29 M  $Na^+$  in NaGlu buffer  $k_{obs}$  increases linearly with  $[RNAP]$  up to the highest accessible concentration ( $\sim 120$  nM), indicating (eq 2) that  $K_1[RNAP] \ll 1$ . In this limit, the overall association rate constant was determined using the following equation:

$$k_a = k_{obs} / [RNAP] (1 + K_1 [RNAP]) \approx k_{obs} / [RNAP] \quad (3)$$

The quality of the approximation was estimated by linear extrapolation of the log-log plots of  $K_1$  vs.  $[RNAP]$  (Fig 4A below) and found to be appropriate.

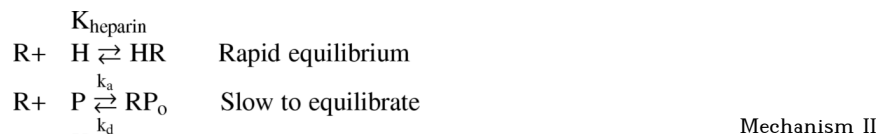
### Determination of the Composite Dissociation Rate Constant $k_d$

- i. The observed rate constant  $k_d$  for the irreversible dissociation of open complexes was determined by fitting  $\theta_t^{open}$  versus time at a given  $[Na^+]$  to a single-exponential decay equation

$$\theta_t^{open} = \theta_{t=0}^{open} e^{-k_d t} \quad (4)$$

where  $\theta_{t=0}^{open}$  is the value of  $\theta_t^{open}$  at time  $t = 0$ .

- ii. The promoter dissociation rate constant ( $k_d$ ) and the RNAP-heparin binding constant ( $K_{heparin}$ ) at 25 °C in  $Glu^-$  and  $F^-$  buffers were determined from the observed decay to equilibrium (relaxation) rate constant  $k_r$  (see below) and the RNAP-promoter association rate constant  $k_a$  (Table1). The data were modeled using the following mechanism:



In mechanism II, H is heparin, P is promoter DNA, R is free RNAP and  $RP_o$  is the final open complex (concentrations of intermediates are negligible).  $K_{heparin}$  is the equilibrium constant for the formation of a heparin-RNAP complex; this equilibrates rapidly on the time scale of association of RNAP with promoter DNA. The composite rate constants for formation ( $k_a$ ) and dissociation ( $k_d$ ) of  $RP_o$  are defined by eqs 2 and 4, respectively. Our analysis of Mechanism II assumes one heparin binding site on RNAP and applies to conditions where  $[H]_{total} \gg [R]_{total} \gg [P]_{total}$ . For this situation, the experimentally determined approach-to-equilibrium rate constant

$k_r = \left( \frac{d \ln (\theta_{t=\infty}^{open} - \theta_t^{open})}{dt} \right) = k_a [R] + k_d$ , where  $[R]$  is the free RNAP concentration.  $[R]$  is constant in these assays (though not in excess over promoter) because the heparin-binding equilibrium buffers its free concentration. The integrated form of this equation is used to determine  $k_d$ :

$$\theta_t^{open} = \frac{k_a [R] (1 - e^{-(k_a [R] + k_d)t})}{k_a [R] + k_d} \quad (5)$$

where [R] is determined from eq 6:

$$[R] = \frac{[R]_{total}}{(1 + K_{heparin}[H]_{total})} \quad (6)$$

For the set of relaxation data collected as a function of  $[H]_{total}$  at a given  $Na^+$  in  $Glu^-$  or  $F^-$  buffer, data at each [heparin] were fit to eqs 5-6, using the value of  $k_a$  determined from the independent kinetics of association experiments (Table 1). Reported values of  $K_{heparin}$  and  $k_d$  for each salt condition represent the average and standard deviation from these individual fits.

## Results

### Single Exponential Kinetics of Formation of E. coli RNA Polymerase – $\lambda P_R$ Promoter Complexes: Effects of Glutamate and Chloride Salts

To compare the effects of the laboratory anion chloride ( $Cl^-$ ) and the physiological anion glutamate ( $Glu^-$ ) on the binding of E. coli RNAP to the  $\lambda P_R$  promoter to form a closed complex and on the subsequent DNA opening step, we determined the kinetics of association over wide ranges of RNAP concentration (1 nM – 100 nM) and concentrations of chloride and glutamate salts (0.13 M to 0.27 M  $Na^+$  in  $Cl^-$  buffer; 0.23 M to 0.64 M  $Na^+$  in  $Glu^-$  buffer) at 25 °C. A limited number of association experiments were performed in  $F^-$  buffer at low [RNAP] to compare to the results in  $Glu^-$  buffer. Sodium salts were used because complexation of potassium by heparin interferes with the heparin challenge (see Methods) at high concentrations of potassium salts (12);  $Mg^{2+}$  was omitted because it is complexed by glutamate (30). In most cases the full accessible range of RNAP and of salt concentration were investigated.

Following either manual or rapid mixing, nitrocellulose filter binding was used to determine the kinetics of formation of long-lived, competitor-resistant complexes ( $RP_o$ ). Representative kinetic data for selected low and high RNAP concentrations over the range of NaCl and NaGlu concentrations are plotted as the fraction of promoter DNA in open complexes ( $\theta_t^{open}$ ) as a function of time in Figures 1 and 2, respectively. The plateau at  $\theta_t^{open} = 1$  observed at long times for all salt concentrations investigated demonstrates that open complex formation is irreversible and therefore directly interpretable in terms of the forward rate constant  $k_{obs}$  (see eq 1 in Methods), without the need for a decay-to-equilibrium analysis. Irreversibility of the forward kinetics is confirmed by direct measurement of the dissociation rate constant (see below).

Single exponential fits of these data to the irreversible first order rate eq 1 (Methods) are shown in Figs 1 and 2. Values of  $k_{obs}$  determined from these fits are given in Supplemental Tables 1 and 2, respectively. To expand the initial (ms) time regime and examine whether the short time data provide any indication of a second (faster) decay, the insets to the panels of Figs 1 and 2 plot the same data as  $\theta_t^{open}$  vs.  $\log t$  (cf. (1,2)). For the  $\lambda P_R$  promoter and the conditions investigated previously (cf. (11,12,20,22)) and in the present study, all association kinetic data are well-described as single exponential decays. Single exponential kinetics of open complex

formation indicate that the step forming the first kinetically significant intermediate ( $I_1$ ) rapidly equilibrates with free promoter DNA on the time scale of the conversion of  $I_1$  to  $I_2$  (21).

### The Observed Forward Rate Constant $k_{obs}$ is a Hyperbolic Function of [RNAP] over the Accessible Range (1 nM to 100 nM)

Values of the overall rate constant  $k_{obs}$  are plotted versus RNAP concentration in Fig 3A ( $Cl^-$ ) and B ( $Glu^-$ ) for the salt concentrations investigated. In most cases these data cover a 100-fold range of RNAP concentrations (~1 nM to 100 nM). At all salt concentrations investigated, except the highest [ $Glu^-$ ], values of  $k_{obs}$  exhibit the expected hyperbolic dependence on [RNAP] (eq 2). Except at the highest salt concentrations, a well-defined plateau is obtained in the accessible range of [RNAP]. There is no evidence of sigmoidicity in any these plots at low [RNAP], as would be predicted if dissociation of holoenzyme into sigma subunit and core polymerase were significant at these concentrations of RNAP and salt (31). The observations of single-exponential association kinetics (Figs 1 & 2) and hyperbolic dependences of  $k_{obs}$  on [RNAP] (Fig 3) validate the use of eq 2 (Methods) to analyze the dependence of  $k_{obs}$  on [RNAP] and obtain  $k_2$ , the DNA opening rate constant and  $K_1$ , the equilibrium constant for forming  $I_1$  (see Methods).

### DNA Opening by RNAP is Relatively Slow and Only Weakly [Salt]-Dependent; Replacing $Cl^-$ by $Glu^-$ Has No Significant Effect on $k_2$ or on its log-log derivative $Sk_2$

Rate constants  $k_2$  of the DNA opening step are plotted on a log-log scale as a function of [ $Na^+$ ] for experiments in  $Cl^-$  and  $Glu^-$  buffer in Fig 4. Values of  $k_2$  decrease very modestly with increasing salt concentration, from  $0.35 s^{-1}$  at 0.15 M  $Na^+$  in  $Cl^-$  buffer to  $0.18$  at 0.29 M  $Na^+$  in  $Glu^-$  buffer, corresponding to time constants of 3-5 s for opening. Neither  $k_2$  at 0.23 M salt (the overlap concentration in our experiments) nor  $Sk_2$  is affected by replacement of  $Cl^-$  by  $Glu^-$  (Fig 4B); individual fits of these data yield  $Sk_2$  values of  $-1.1 \pm 0.1$  and  $-0.9 \pm 0.3$  in  $Cl^-$  and  $Glu^-$  buffers, respectively. As shown in Fig 4A, the combined data fall on a common line with a log-log slope of  $Sk_2 = -1.1 \pm 0.1$ . Previously we found from [ $KCl$ ]-upshift experiments at 10 and 37 °C in transcription buffer (10 mM  $MgCl_2$ ) that the rate constant  $k_{-2}$  for the reverse direction of this step ( $I_2$  to  $I_1$ ) is independent of [ $KCl$ ] ( $Sk_{-2} = 0$ ; (24)). Interpolation between values yields  $k_{-2} \approx 1.7 s^{-1}$  at 25 °C. Assuming this value of  $k_{-2}$  applies to the [salt] conditions investigated here, we obtain equilibrium constants  $K_2$  for DNA opening by RNAP (i.e.  $I_1 \rightleftharpoons I_2$ ) that decrease from 0.2 at 0.15 M salt to 0.1 at 0.29 M salt.  $I_2$  is therefore unstable with respect to  $I_1$  at all salt concentrations, and the [salt]-dependence of the DNA opening step  $I_1 \rightleftharpoons I_2$  on the protein is small ( $SK_2 = Sk_2 - Sk_{-2} = -1.1 \pm 0.1$ ).

### Formation of Wrapped $I_1$ Is Strongly [Salt]-Dependent ( $SK_1 = -6.9 \pm 0.3$ ); Replacing $Cl^-$ by $Glu^-$ Increases $K_1$ ~30-fold Without Significantly Affecting $SK_1$

The proposed RNAP-DNA interface in  $I_1$  spans 100 bp; the net positive charge on RNAP in this interface is at least +37 (see Discussion). How [salt]-dependent is this binding interaction? In  $Cl^-$  buffer the binding constant  $K_1$  for formation of  $I_1$  decreases from  $1.8 \times 10^8 M^{-1}$  at 0.15 M  $Na^+$  to  $9.9 \times 10^6 M^{-1}$  at 0.23 M  $Na^+$ . In  $Glu^-$  buffer at 0.23 M  $Na^+$ ,  $K_1$  is  $3.6 \times 10^8 M^{-1}$  and decreases to  $8 \times 10^7 M^{-1}$  at 0.29 M  $Na^+$ . In both  $Cl^-$  and  $Glu^-$ ,  $\log K_1$  decreases linearly with  $\log[Na^+]$  with slopes  $SK_1 = d\log K_1/d\log[salt]$  which are the same within uncertainty ( $SK_1 = -6.8 \pm 0.3$  in  $Cl^-$ ,  $SK_1 = -7.5 \pm 2.3$  in  $Glu^-$ ; see Fig 4A and Table 1). Fitting both data sets together yields  $SK_1 = -6.9 \pm 0.3$ . These are large [salt]-dependences, but not nearly as large as expected from consideration of the interface (see Discussion).

At 0.23 M  $Na^+$ , the only salt concentration where the data sets overlap, the value of  $K_1$  in  $Glu^-$  buffer exceeds that in  $Cl^-$  by a factor of ~30. This is the same factor by which the log-log plots of  $k_a$  vs. [ $Na^+$ ] in Fig 4B are displaced. Such a large effect of replacing  $Cl^-$  with



$\text{Glu}^-$  on  $K_1$  is likely a Hofmeister salt effect, based on the observation that fluoride and glutamate have very similar effects on  $k_a = K_1 k_2$ , as well as on  $k_d$  (see below).

### Replacement of $\text{Cl}^-$ by $\text{Glu}^-$ Increases the Second-Order Association Rate Constant $k_a$ by ~30-fold at All [Salt]

Above 0.23 M  $\text{Na}^+$  in  $\text{Cl}^-$  buffer and 0.29 M  $\text{Na}^+$  in  $\text{Glu}^-$  buffer, the equilibrium constant  $K_1$  for  $I_1$  formation becomes too small to allow us to dissect  $k_{\text{obs}}$  into  $K_1$  and  $k_2$ . At higher [salt], we find that  $k_{\text{obs}}$  increases linearly with [RNAP], as shown in Fig 3B in  $\text{Glu}^-$  buffer at 0.55 M  $\text{Na}^+$ . Linearity indicates that  $K_1[\text{RNAP}] \ll 1$  over the accessible range of [RNAP]. In this limit, the second order association rate constant  $k_a = k_{\text{obs}}/[\text{RNAP}](1 + K_1[\text{RNAP}]) \approx k_{\text{obs}}/[\text{RNAP}]$ , where the quality of the last approximation can be estimated by extrapolation of the log-log plots of  $K_1$  vs. [RNAP] (Fig 4A). Although individual values of  $K_1$  and  $k_2$  cannot be determined in this higher [salt] range, measurements of  $k_{\text{obs}}$  at low [RNAP] (typically 7 nM) were performed in  $\text{Cl}^-$ ,  $\text{Glu}^-$  and  $\text{F}^-$  buffers up to the highest  $[\text{Na}^+]$  accessible in each to test for curvature of the log-log plots arising from Hofmeister effects (32). All determinations of  $k_a$  are listed in Table 1, and plotted in Fig 4B as a log-log plot together with those obtained from the data of Fig 3. A much wider range of high  $[\text{Na}^+]$  can be investigated in  $\text{Glu}^-$  and  $\text{F}^-$  buffers because  $k_d$  is much smaller in  $\text{Glu}^-$  and  $\text{F}^-$  buffers than in  $\text{Cl}^-$ . Over the full range of  $[\text{Glu}^-$  (or  $\text{F}^-)]$  investigated,  $k_a$  decreases by more than three orders of magnitude (from  $7.3 \times 10^7 \text{ M}^{-1} \text{ s}^{-1}$  at 0.23 M  $\text{Na}^+$  to  $2.6 \times 10^4 \text{ M}^{-1} \text{ s}^{-1}$  at 0.64 M  $\text{Na}^+$ ). These log-log plots are linear and parallel within the uncertainty over the entire accessible salt range in both  $\text{Cl}^-$  ( $S_{k_a} = -8.0 \pm 0.2$ ) and  $\text{Glu}^-/\text{F}^-$  ( $S_{k_a} = -8.3 \pm 0.2$ ). The offset corresponds to ~30-fold faster association in  $\text{Glu}^-$  than in  $\text{Cl}^-$ . This difference is entirely the result of the difference in  $K_1$ .

### Disassembly of the RNAP Clamp/Jaw in Dissociation of $\text{RP}_0$ Complexes in $\text{Glu}^-$ is Remarkably Slower and Much Less [Salt] Dependent than in $\text{Cl}^-$

Dissociation kinetic studies probe the steps of disassembly of the clamp/jaw (conversion of  $\text{RP}_0$  to  $I_2$ ) and DNA closing (conversion of  $I_2$  to  $(I_1-I_2)^\ddagger$ ). Irreversible dissociation data at 25 °C in 0.23 M – 0.29 M  $\text{Na}^+$  in  $\text{Cl}^-$  buffer are plotted in Fig 5 as  $\theta_t^{\text{open}}$  vs. time, and fit to a single exponential decay equation (eq 4). To show the quality of these single exponential fits, the inset in Fig 5 plots  $\theta_t^{\text{open}}$  vs  $\log t$ ; essentially 100% of the decay is described by the fit with dissociation rate constant  $k_d$ . This indicates that the steps that convert the final open complex  $\text{RP}_0$  to the kinetically significant, open intermediate  $I_2$  rapidly equilibrate on the time scale of the dissociation-rate-determining conversion of  $I_2$  to the closed intermediate  $I_1$ . ( $I_1$  is not filter-retainable in the presence of heparin.) Values of  $k_d$  increase by an order of magnitude with this 25% increase in salt concentration (from  $2.9 \times 10^{-4} \text{ s}^{-1}$  at 0.23 M  $\text{Na}^+$  to  $2.4 \times 10^{-3} \text{ s}^{-1}$  at 0.29 M  $\text{Na}^+$ ); these are plotted on a log-log scale vs  $[\text{Na}^+]$  in Fig 7 below. The plot is linear with slope  $S_{k_d} = 9.2 \pm 0.1$ , consistent with a previous determination for this promoter in its natural context (12).

By contrast, dissociation in  $\text{Glu}^-$  is extraordinarily slow at 25 °C and much less dependent on salt concentration. Attempts to directly determine  $k_d$  at 0.33 M and 0.6 M  $\text{Na}^+$  in  $\text{Glu}^-$  buffer, using a very high competitor concentration (2.5 mg/mL heparin) in an attempt to ensure irreversibility, exhibited very slow dissociation with rate constants in the range  $10^{-5}$  to  $10^{-6} \text{ s}^{-1}$ , orders of magnitude slower than in  $\text{Cl}^-$  at lower [salt] (Fig 7). Permanganate footprinting of these 25 °C promoter complexes as a function of  $[\text{Na}^+]$  in  $\text{Glu}^-$  buffer shows them to be open in the vicinity of the transcription start site over the range 0.13 M to 0.6 M  $\text{Na}^+$  (TG, unpublished).

As an alternative, faster and more robust method to determine  $k_d$  at 25 °C as a function of  $[\text{Na}^+]$  in  $\text{Glu}^-$  buffer, we observed the kinetics of approach to promoter binding equilibrium in experiments performed at very low, constant [RNAP], maintained by using heparin as an

RNAP buffer. In these experiments, RNAP was initially equilibrated with excess heparin, and subsequently mixed with promoter DNA to initiate open complex formation, which is reversible in excess heparin because the free [RNAP] is so low.

Representative results at 0.46 M Na<sup>+</sup> in Glu<sup>-</sup> buffer are shown in Fig 6 as plots of  $\theta_t^{\text{open}}$  as a function of time for different heparin concentrations. In these experiments,  $[\text{heparin}]_{\text{total}} \gg [\text{RNAP}]_{\text{total}} \gg [\text{promoter}]_{\text{total}}$ . The free [RNAP] is very small (generally  $[\text{RNAP}]_{\text{free}} < [\text{promoter DNA}]_{\text{total}}$  see supplemental Table 3) because almost all RNAP is bound to heparin under the conditions of these experiments. Though not in excess, the free [RNAP] is constant throughout the time course of reversible association because it is buffered by the heparin-binding equilibrium. The heparin binding equilibrium is found to be established rapidly on the time scale of the promoter binding equilibrium, which takes many hours, so the observed kinetics are entirely the approach to equilibrium of promoter binding. The first order rate constants obtained from single exponential fits to these data (see Methods) are relaxation rate constants  $k_r$ , which are the sum of the pseudo-first order (constant RNAP concentration) association rate constant ( $k_a[\text{R}]_{\text{free}}$ ) and the dissociation rate constant  $k_d$  (see Supplemental Table 3). Hence these decay-to-equilibrium experiments are less time-consuming than direct dissociation experiments. To obtain an accurate value for  $k_d$  from  $k_r$ , independently-determined values of  $k_a$  at each of these [Na<sup>+</sup>] in Glu<sup>-</sup> and F<sup>-</sup> buffers (Table 1) were used. Consequently  $k_d$  is well-determined, especially for conditions where  $k_d \geq k_a[\text{R}]_{\text{free}}$ .

Values of  $k_d$  obtained from the analyses of the data of Fig 6 and comparable series of reversible polymerase-promoter binding experiments performed over a range of [Na<sup>+</sup>] in Glu<sup>-</sup> and F<sup>-</sup> buffers are tabulated in Table 2 and plotted in Fig 7 as a log-log plot vs. [Na<sup>+</sup>] to compare with the behavior of  $k_d$  in Cl<sup>-</sup> buffer. Values of  $k_d$  in Glu<sup>-</sup> and F<sup>-</sup> buffers fall on a common line on this log-log plot, greatly offset from  $k_d$  values in Cl<sup>-</sup> buffer, and with a much shallower slope ( $S_{k_d} = 3.2 \pm 0.8$  for Glu<sup>-</sup>/F<sup>-</sup> vs.  $S_{k_d} = 9.2 \pm 0.1$  for Cl<sup>-</sup>).

At 0.31 M Na<sup>+</sup>, the salt concentration requiring the least extrapolation of the data sets in Fig 7,  $k_d$  is  $\sim 10^3$ -fold larger in Cl<sup>-</sup> than in Glu<sup>-</sup> or F<sup>-</sup> buffers. This ratio is predicted to increase with increasing salt concentration if the log-log plot remains linear in Cl<sup>-</sup> buffer. These differences in magnitude and log-log salt derivative of  $k_d$  between Cl<sup>-</sup> and F<sup>-</sup> or Glu<sup>-</sup> are very large, exceeding those previously observed for equilibrium/rate constants of other protein processes, and also contrast with the behaviors seen in Fig 4 for  $K_1$ ,  $k_2$ , and  $k_a$  (see Discussion), indicating that very different conformational changes and interfaces are involved in these different steps.

For all determinations of  $k_d$  from  $k_r$ , the constant free [RNAP] at each [heparin] investigated is also obtained. Values of the free [RNAP] range from  $\sim 10^{-12}$  M at low [Na<sup>+</sup>] and high [heparin] to  $\sim 10^{-10}$  M at high [Na<sup>+</sup>] and low [heparin]. Analysis of these decay to equilibrium experiments as a function of heparin concentration at constant salt concentration provides no evidence for subunit dissociation of RNAP holoenzyme at any condition investigated. From these free [RNAP], values of the heparin binding constant  $K_{\text{heparin}}$  are obtained at each [Na<sup>+</sup>] investigated in Glu<sup>-</sup> and F<sup>-</sup> buffers. Values of  $K_{\text{heparin}}$  are plotted as a log-log plot vs. [Na<sup>+</sup>] in Fig 8. In Glu<sup>-</sup> and F<sup>-</sup> buffers, the [salt] dependence of  $K_{\text{heparin}}$  ( $S_{K_{\text{heparin}}} = -13 \pm 0.2$ ) is similar to that of the RNAP-promoter binding constant ( $S_{K_{\text{obs}}} = S_{k_a} - S_{k_d} = -(8.3 \pm 0.2) + (3.2 \pm 0.8) = 11.5 \pm 1.0$ ).

## DISCUSSION

Here we propose interpretations of the effects of [salt] and the difference between effects of Glu<sup>-</sup> and F<sup>-</sup> versus Cl<sup>-</sup> on the steps of open complex formation in terms of extant structural and thermodynamic characterizations of each step. Qualitative comparisons are also made with

the effects of these salts on other protein-DNA interactions, on protein folding and DNA melting, and on model processes. Both the similarity of the effects of  $\text{Glu}^-$  and  $\text{F}^-$  and the large differences between effects of these anions and of  $\text{Cl}^-$  on the early and late steps of open complex formation indicate that these are Hofmeister effects and that they arise from greater exclusion of  $\text{Glu}^-$  and  $\text{F}^-$  than of  $\text{Cl}^-$  from nonpolar hydrocarbon surface, as proposed for protein folding (19) and for IHF-H'DNA binding (32). Fig 9 presents an overview of the steps, proposed conformational changes and the effects of [salt] and anion on each. We discuss how the  $\text{Glu}^-$  results here are predicted to affect  $\sigma^{70}$  holoenzyme interactions at strong promoters *in vivo* during the adaptation to an osmotic upshift.

### Opening of the Initiation Bubble (-11 to +2) in the Active Site Cleft is Surprisingly Insensitive to [Salt] and Anion: Implications for Regulation of $\text{RP}_0$ Formation

In many biochemical processes, including enzyme catalysis and active transport, rapidly reversible initial and final steps bracket a bottleneck step that performs the key biological function (e.g. catalysis/transport). In these cases, regulation is largely achieved by effects of ligands or solutes on the rapidly reversible initial and final steps, but not on the key central catalytic/transport step of the mechanism. In  $\text{RP}_0$  formation, the first and last steps rapidly equilibrate on the time scale of the cooperative DNA opening step (24). Here and in our previous work, we find large effects of [salt], anion and solutes on the initial and final steps, but *not* on the central bottleneck step that converts the closed complex  $\text{I}_1$  to the unstable open complex  $\text{I}_2$ . An exception is the action of far upstream DNA as an effector ligand. Truncation of DNA upstream of -47 greatly reduces the opening rate because it reduces the extent of insertion of downstream duplex DNA in the active site cleft in  $\text{I}_1$ , thereby changing the nature of this intermediate (33).

Such a regulatory strategy would appear to be well-suited to organisms like *E. coli* that grow over a wide range of solution conditions, or in general to any cell responding to changes in environment. Clearly in order to reprogram genetic expression, DNA opening is required irregardless of solution conditions in the cell. The response to changes in growth conditions utilizes differences in promoter sequence, and/or shifts in the concentrations of sigma factors, "feedback" solutes (KGlu), and stress factors (ppGpp). It will be important to determine whether these factors act to increase or decrease levels of  $\text{I}_1$  or  $\text{I}_2$ , leaving the opening step unaffected, or whether they affect structural features of  $\text{I}_1$  or  $\text{I}_2$  which are central for DNA opening.

The small magnitude of the [salt] dependences of both rate constants of the DNA opening step ( $\text{Sk}_2 = -1$ ,  $\text{Sk}_{-2} = 0$ ,  $\text{SK}_2 = -1$ ) contrast with the situation for DNA melting in solution, which is significantly more strongly [salt] dependent (25). Indeed this small [salt] dependence of DNA opening by RNAP appears inconsistent with proposed mechanisms based on structural data in which DNA opening occurs outside (above) the active site channel (34-36). To explain the small salt dependence of opening in the active site cleft, we propose that these very small effects of [salt] on a process (DNA opening) which is strongly [salt]-dependent in solution may indicate that the backbones of both DNA strands interact with polymerase throughout the process, and/or that compensation is present between ion uptake and release. Possibly loading DNA as a duplex in the highly positively charged cleft in  $\text{I}_1$  (see above) neutralizes the charge in the region (-11 to +2) opened in forming  $\text{I}_2$ . The subsequent movement of the template strand into the active site might then involve an exchange for basic contacts at the top of the cleft to those at the bottom, thereby buffering it from changes in [salt]. Compensations in the exchange between region 1.1 and the single strands in the channel (as well as unwrapping upstream DNA) may lead to small net changes in ASA, which in turn result in a small net change in binding free energy for the formation of  $\text{I}_2$  from  $\text{I}_1$ . In addition, opening occurs in a

deep cleft that is bounded by highly conserved structural features on the large subunits (37), which may in some way isolate the process from the bulk solution.

For the  $\lambda P_R$  promoter at typical [salt], the initial open complex  $I_2$  is unstable relative to  $I_1$  at low temperatures (<15 °C), highly unstable relative to  $RP_o$  at higher temperatures (24), and therefore is only transiently populated at any temperature. Binding free energy (specifically a favorable entropy change, since the net enthalpy change for conversion of  $I_1$  to  $I_2$  is +25; (22,24)) drives the opening of the DNA in the channel. However, the small magnitude of  $SK_2$  indicates that ion release is not the origin of the favorable entropy change for this step.

While the thermodynamic origins of this driving force remain unclear, we propose the following series of structural events drive opening in the conversion of  $I_1$  to  $I_2$ . Repositioning of  $\sigma$  region 1.1 in response to loading duplex DNA in the cleft in  $I_1$  allows the strands to descend further the channel in  $(I_1-I_2)^\ddagger$ , increasing the bending distortion at -12/-11. This change likely exposes bases in the -10 hexamer on the NT strand (38) which are “captured” by the conserved aromatic side chains on region 2 of sigma (39-42). Additionally, a gradient of positive charge may exist in the channel, increasing from the top to the bottom. Such a distribution of lysines and arginines could help bring the template strand down to the base of the cleft once region 1.1 has moved.

For the entire bubble to open, we propose that a highly conserved region on the downstream lobe of  $\beta$  known as fork loop 2 (T. thermophilus (T. th.) 413-430, E. coli 533-550; (37)) may insert in the minor groove of the DNA duplex, as the DNA descends, prying apart the strands and helping to stabilize the open bubble surrounding +1. By analogy with base flipping enzymes, this insertion would further unwind the helix and create an additional  $\sim 90^\circ$  bend near -2/-1. In the crystal structure of the T. th. transcription elongation complex, fork loop 2 is positioned between the nontemplate strand and the backbone of the RNA product (43).

### **Conversion of the Unstable Open Complex $I_2$ to the Stable Open Complex $RP_o$ : Evidence for Large-Scale Folding and Assembly of a Clamp/Jaw on Downstream DNA**

The finding here that replacement of  $Cl^-$  by  $Glu^-$  (or  $F^-$ ) greatly increases the lifetime of  $RP_o$  at 25 °C, especially at higher  $[Na^+]$  is most consistent with a large-scale burial of hydrocarbon surface in the late steps (from which  $F^-$  and  $Glu^-$  are more completely excluded than is  $Cl^-$  (19)). This work along with our previous studies of  $k_d$  as a function of temperature, KCl, urea, and glycine betaine all indicate that large-scale rearrangements occur in the late steps of forming  $RP_o$  (24,27). These steps exhibit a large negative heat capacity change (-1 kcal/K), comparable to that for folding a 75-100 residue globular protein; the effect of urea is consistent with folding at least 100 residues, while the effects of [salt] and GB are consistent with formation of a significant new RNAP-DNA interface involving 10-15 DNA phosphates. The most plausible scenario is that >100 residues in RNAP fold and bind to the downstream DNA backbone in the conversion of  $I_2$  to  $RP_o$  (24,27).

From an analysis which predicts natively disordered regions in E. coli RNAP, we deduced that the regions that fold are parts of the downstream clamp and jaw of  $\beta'$  (27). Highly conserved in bacterial RNAP (37), the following are positioned near the downstream DNA (+5 to +20) in the FRET model of  $RP_o$  (44) and the TEC structure (43): (i) a highly positively charged helix-hairpin-helix (T. th. 470-507, E. coli 194-232), (ii) a C-terminal region (T. th. 1378-1424, E. coli 1263-1310) adjacent to (i) and switch 5 (37); and (iii) the mobile downstream jaw (T. th. 1270-1329, E. coli 1142-1214). Regions (i) and (ii) form part of the ‘clamp’ of RNAP. Strong biochemical evidence exists for interactions between the clamp and jaw and downstream DNA in  $RP_o$ . Internal deletions in the jaw (45) as well as binding of the negatively charged phage protein Gp2 (46) to the jaw strongly destabilize  $RP_o$  at various promoters including  $\lambda P_R$ . The helix-hairpin-helix binds near the major groove at +10 in the TEC; deletion

of *E. coli* 210-215 also strongly destabilizes  $RP_o$  (47). The lineage-specific sequence insertion 3 (SI3) in *E. coli*  $\beta'$  (48) likely also plays a part in the assembly of the stabilizing clamp/jaw. Comprised of a repeated sandwich-barrel-hybrid motif,  $\beta'$ SI3 connects to the “trigger loop” by a flexible 13 amino acid linker (49). Deletion of  $\beta'$ SI3 increases  $k_d$  at  $\lambda P_R$  by ~4 fold (27). In a model of the TEC,  $\beta'$ SI3 is positioned near the jaw, the downstream lobe of beta and the downstream DNA from +13 to +18 (49).

We proposed that the clamp and jaw domains are mobile and partially disordered in  $I_2$  and assemble on the downstream DNA in the conversion of  $I_2$  to  $RP_o$  (27). Because the regions in the clamp/jaw contain runs of positive residues, their interactions with duplex DNA are predicted to release cations. Importantly, our data indicate that the RNAP machinery clamps onto the downstream DNA during  $I_2 \rightarrow RP_o$ , after the entire transcription bubble has been untwisted and opened in the active site channel ( $I_1 \rightarrow I_2$ ; Gries et al., unpublished).

### Predicting the Salt Concentration Dependence of Forming the 100 bp Wrapped DNA Interface in the Closed Intermediate $I_1$

The first steps of  $RP_o$  formation discriminate promoter from nonpromoter DNA by establishing interactions between sigma regions 4 and 2 and conserved six bp sequences at -35 and -10, respectively (41). However, formation of  $I_1$  at the  $\lambda P_R$  promoter creates an extensive interface with DNA that extends well beyond the -10 and -35 regions: protection from hydroxyl radical ( $\bullet OH$ ) or DNase I cleavage of the DNA backbone in  $I_1$  extends to at least +20 at  $\lambda P_R$  (23,50) (and at the  $\lambda P_{RM up1}$  promoter (51)); upstream protection from  $\bullet OH$  cleavage at  $\lambda P_R$  extends to ~-85 (23) (also apparently at the T7A1 promoter (2)). These data, interpreted using structures of the free RNAP (35,52) and a complex with a fork junction DNA (from -7 to -41; (34)), are most simply consistent with a model (23) where upstream DNA is wrapped around RNAP and downstream DNA is bound in the active site channel created by the opposition of the  $\beta$  and  $\beta'$  subunits (footnote 1). What is the relationship between this model of  $I_1$  and  $SK_1$ ?

In our model of  $I_1$ , approximately sixty-two positive (arginine (R), lysine (K), histidine (H)) and twenty-five negative (aspartate (D), glutamate (E)) side chains lie near the DNA phosphate backbone, yielding a net charge of ~+37. With the exception of the C-terminal domain (CTD) of  $\alpha$  (modeled using the crystal structure of the *E. coli* subunits (53)), this charge count is based on the *T. th.* RNAP subunits ( $\alpha NTD$ ,  $\beta$ ,  $\beta'$ ,  $\omega$ ,  $\sigma^A$ ). However, the charged residues involved in forming the interface from -55 to +20 are highly conserved in bacterial RNAP. With the exception of three (R, K, H) and three (D, E) on  $\beta$  predicted to contact DNA from -11 to +5 in the model of  $I_1$ , the remainder from the count above (R, K, H, E, D) are present in *E. coli*. While the one-to-one correspondence for charged residues in the region upstream of -55 is more variable between *T. th.* and *E. coli*, the overall charge distribution near the upstream wrapping track (-70 to -85) appears relatively conserved. This approximate structural estimate provides a reasonable basis for predicting the contribution from neutralization of DNA phosphate charge to the observed [salt] dependence of  $I_1$  formation. For binding of an oligocation ligand with a charge of +37 to DNA, the predicted low-[salt] value of  $SK_{obs}$  is approximately -32 (or more negative if ion release from the ligand contributes to  $SK_{obs}$ ).

### Interpretation of the Much Smaller than Expected Effect of [Salt] on $I_1$ Formation

While interactions with the -35 and -10 hexamers involve base specific interactions with  $\sigma^{70}$  regions 4 and 2, respectively, the interface in  $I_1$  is composed of predominantly nonspecific DNA backbone interactions with the other RNAP subunits (e.g.  $\alpha CTDs$ ,  $\beta$  and  $\beta'$ ). Our estimate

---

While our data do not allow us to determine the order of formation of these interactions, they have been determined by fast hydroxyl radical footprinting of early complexes at the T7A1 promoter (1,2). At T7A1, interactions are first established upstream and then proceed downstream (2). These early intermediates at  $\lambda P_R$  rapidly equilibrate with one another and thus are not separated in the kinetic analysis.

of  $SK_1$  ( $\sim -30$  (above)) is much larger in magnitude than the observed log-log dependence of  $K_1$  on  $[Na^+]$  ( $SK_1 \sim -7$  in both  $Cl^-$  and  $Glu^-$  buffers). This difference suggests that some process involving extensive salt ion uptake by RNAP has evolved to largely compensate for this predicted cation release from the promoter DNA in forming  $I_1$  from free RNAP and promoter DNA. We propose two scenarios involving cation uptake that may occur in  $I_1$  formation: disruption of surface salt bridges on RNAP coupled to forming the interface (32, 54,55), and the placement of duplex DNA next to negatively charged region 1.1 in the channel.

Given the juxtaposition of negative and positive charges in the upstream half of the  $I_1$  interface, we propose that coupled salt bridge disruption acts to reduce the binding constant  $K_1$  and the magnitude of its log-log salt derivative  $|SK_1|$ , and likely explains the large negative  $\Delta C_p$  of this step ( $-1.4 \text{ kcal M}^{-1} \text{ K}^{-1}$ ; (22)). However, the walls and floor DNA active site channel of RNAP are highly basic. Given this charge distribution, it seems unlikely that salt bridge disruption could offset the salt ion release from binding  $>20$  bp of downstream duplex in the channel. What does?

In free  $\sigma^{70}$  RNAP, the highly negatively charged region 1.1 lies in the active site channel (44). Where is it in  $I_1$ ? Solute probes of changes in anionic (GB) and amide (urea) surface area do not detect any signature of release of sigma region 1.1 in forming  $I_1$  (27). Instead, our estimates of the burial of anionic and amide surface in the  $I_1$  protein-DNA interface based on structural data are completely consistent with the magnitude of effects of glycine betaine and urea on  $K_1$ . As a result, we proposed that it was most likely that region 1.1 is not expelled during the formation of  $I_1$ , remaining bound and masking the active site (27). It seems likely that any cation release from loading of duplex DNA in the channel must be offset by cation uptake as a result of placing the two highly negatively charged regions next to each other.

In the model of  $I_1$ , DNA downstream of +1 lies above region 1.1 (23,27). Region 1.1 has a net charge of  $-19$  and can be modeled as a negatively charged alpha-helical “plug” at the N-terminus (56) followed by an unstructured, negatively charged coil. We speculate that positioning downstream duplex DNA next to this negatively charged single stranded (ss) DNA mimic may be somewhat analogous to DNA triplex formation. Theoretically the limiting law per charge ion association is 0.76 for ss DNA, 0.88 for double stranded (ds) DNA, increasing to 0.92 in a triplex (ts). If this model is appropriate for placing 20 bp of duplex DNA near sigma region 1.1, then we predict approximately five cations are taken up.

### Implications of Effects of $Glu^-$ on the Steps of Initiation for Adaptation to Osmotic Stress in vivo

In vitro, Gralla observed that transcription from open complexes at the strong  $\sigma^{70}$  promoter lacUV5 decreases greatly as the K $Glu$  concentration is increased from 0.1 to 0.4 M (9). If  $Cl^-$  were the cytoplasmic anionic osmolyte, such increases in  $K^+$  concentrations would cause dissociation of RNAP and many other proteins from nucleic acids. However, in  $Glu^-$ , open complexes at the strong  $\lambda P_R$  promoter are unexpectedly long-lived over the entire range of [salt] investigated here, ( $k_d < 10^{-5} \text{ s}^{-1}$  at 25 °C even at 0.5 M  $Glu^-$ , corresponding to a lifetime ( $1/k_d$ ) of open complexes exceeding one day). These data suggest that open complexes at strong  $\sigma^{70}$  promoters in vivo (where negative supercoiling should also favor  $RP_o$  formation) do not dissociate after an osmotic upshift, but may have difficulty escaping the promoter to transcribe.

While transcription from many  $\sigma^{70}$  holoenzyme-promoter is reduced at high  $Glu^-$ , transcription of osmotically-regulated promoters by  $\sigma^S$  holoenzyme increases (7,8). Intriguingly, in vitro DNase I footprints of  $\sigma^S$  RNAP-osmY promoter complexes reveal that contacts upstream of  $-30$  are lost as  $[KGlu]$  increases, allowing escape from the promoter (9). Gralla and coworkers deduced from these data that high concentrations of  $K^+$  and  $Glu^-$  are able to release  $\sigma^S$  RNAP that are poised at lower salt ion concentrations, allowing both transcription and reinitiation

(9,57,58). By contrast,  $\sigma^{70}$  RNAP appears to remain bound an open promoter complex as [salt] increases in  $\text{Glu}^-$  buffer (this work), but its ability to transcribe is progressively reduced (9). Hence in vivo salt ion concentrations themselves appear capable both of switching transcription from one set of genes to another, and of poisoning RNAP to rapidly start at another set when conditions change (9,58,59).

Gralla and coworkers observe that the ability of an anion to increase  $\sigma^S$  transcription at osmotic genes is correlated with its position in the Hofmeister series (10). Since the exclusion of the Hofmeister anion  $\text{Glu}^-$  from hydrocarbon surfaces causes it to favor processes that reduce the exposure of nonpolar surface to the solution (e.g. folding, assembly, binding) (18), differences in the amounts and types of surface area changes in biological processes will in turn give rise to differential effects of  $\text{Glu}^-$ .

## Supplementary Material

Refer to Web version on PubMed Central for supplementary material.

## Acknowledgments

We thank Alison Huckenpahler for her contributions to the glutamate association kinetic data. We thank the editor and reviewers for their help in revising the manuscript.

## Abbreviations

ASA	water-accessible surface area
GB	glycine betaine
PNAI	protein nucleic acid interactions
RNAP	RNA polymerase
$\sigma^S$	stationary phase sigma factor

## References

1. Rogozina A, Zaychikov E, Buckle M, Heumann H, Sclavi B. DNA melting by RNA polymerase at the T7A1 promoter precedes the rate-limiting step at 37 °C and results in the accumulation of an off-pathway intermediate. *Nucleic Acids Res* 2009;37:5390–5404. [PubMed: 19578065]
2. Sclavi B, Zaychikov E, Rogozina A, Walther F, Buckle M, Heumann H. Real-time characterization of intermediates in the pathway to open complex formation by Escherichia coli RNA polymerase at the T7A1 promoter. *Proc Natl Acad Sci USA* 2005;102:4706–4711. [PubMed: 15738402]
3. Cayley S, Record MT Jr. Roles of cytoplasmic osmolytes, water, and crowding in the response of Escherichia coli to osmotic stress: biophysical basis of osmoprotection by glycine betaine. *Biochemistry* 2003;42:12596–12609. [PubMed: 14580206]
4. Wood JM. Osmosensing by bacteria: signals and membrane-based sensors. *Microbiol Mol Biol Rev* 1999;63:230–262. [PubMed: 10066837]
5. Cayley DS, Guttman HJ, Record MT Jr. Biophysical characterization of changes in amounts and activity of Escherichia coli cell and compartment water and turgor pressure in response to osmotic stress. *Biophys J* 2000;78:1748–1764. [PubMed: 10733957]
6. Gralla JD, Vargas DR. Potassium glutamate as a transcriptional inhibitor during bacterial osmoregulation. *EMBO J* 2006;25:1515–1521. [PubMed: 16541105]
7. Weber A, Jung K. Profiling early osmotic stress-dependent gene expression in Escherichia coli using DNA microarrays. *J Bacteriol* 2002;184:5502–5507. [PubMed: 12218039]

8. Cheung KJ, Badarinarayana V, Selinger DW, Janse D, Church GM. A microarray-based antibiotic screen identifies a regulatory role for supercoiling in the osmotic stress response of *Escherichia coli*. *Genome Res* 2003;13:206–215. [PubMed: 12566398]
9. Lee SJ, Gralla JD. Osmo-regulation of bacterial transcription via poised RNA polymerase. *Mol Cell* 2004;14:153–162. [PubMed: 15099515]
10. Gralla JD, Huo YX. Remodeling and activation of *Escherichia coli* RNA polymerase by osmolytes. *Biochemistry* 2008;47:13189–13196. [PubMed: 19053283]
11. Roe JH, Burgess RR, Record MT Jr. Kinetics and mechanism of the interaction of *Escherichia coli* RNA polymerase with the  $\lambda P_R$  promoter. *J Mol Biol* 1984;176:495–522. [PubMed: 6235375]
12. Roe JH, Record MT Jr. Regulation of the kinetics of the interaction of *Escherichia coli* RNA polymerase with the  $\lambda P_R$  promoter by salt concentration. *Biochemistry* 1985;24:4721–4726. [PubMed: 2934084]
13. Leirimo S, Harrison C, Cayley DS, Burgess RR, Record MT Jr. Replacement of potassium chloride by potassium glutamate dramatically enhances protein-DNA interactions in vitro. *Biochemistry* 1987;26:2095–2101. [PubMed: 2887198]
14. Barkley MD, Lewis PA, Sullivan GE. Ion effects on the lac repressor-operator equilibrium. *Biochemistry* 1981;20:3842–3851. [PubMed: 7272280]
15. Lohman TM, Chao K, Green JM, Sage S, Runyon GT. Large-scale purification and characterization of the *Escherichia coli* rep gene product. *J Biol Chem* 1989;264:10139–10147. [PubMed: 2524489]
16. Dragan AI, Li Z, Makeyeva EN, Milgotina EI, Liu Y, Crane-Robinson C, Privalov PL. Forces driving the binding of homeodomains to DNA. *Biochemistry* 2006;45:141–151. [PubMed: 16388589]
17. Maslak M, Martin CT. Effects of solution conditions on the steady-state kinetics of initiation of transcription by T7 RNA polymerase. *Biochemistry* 1994;33:6918–6924. [PubMed: 7911327]
18. Pegram LM, Record MT Jr. Thermodynamic origin of Hofmeister ion effects. *J Phys Chem B* 2008;112:9428–9436. [PubMed: 18630860]
19. Pegram LM, Wendorff T, Erdmann R, Shkel IA, Bellissimo D, Felitsky DJ, Record MT Jr. Why Hofmeister effects of many salts favor protein folding but not DNA helix formation. *Proc Natl Acad Sci USA*. 2010 in press.
20. Roe JH, Burgess RR, Record MT Jr. Temperature dependence of the rate constants of the *Escherichia coli* RNA polymerase- $\lambda P_R$  promoter interaction. Assignment of the kinetic steps corresponding to protein conformational change and DNA opening. *J Mol Biol* 1985;184:441–453. [PubMed: 3900414]
21. Tsodikov OV, Record MT Jr. General method of analysis of kinetic equations for multistep reversible mechanisms in the single-exponential regime: application to kinetics of open complex formation between  $E\sigma^{70}$  RNA polymerase and  $\sigma P_R$  promoter DNA. *Biophys J* 1999;76:1320–1329. [PubMed: 10049315]
22. Saecker RM, Tsodikov OV, McQuade KL, Schlax PE Jr, Capp MW, Record MT Jr. Kinetic studies and structural models of the association of *E. coli*  $\sigma^{70}$  RNA polymerase with the  $\lambda P_R$  promoter: large scale conformational changes in forming the kinetically significant intermediates. *J Mol Biol* 2002;319:649–671. [PubMed: 12054861]
23. Davis CA, Bingman CA, Landick R, Record MT Jr, Saecker RM. Real-time footprinting of DNA in the first kinetically significant intermediate in open complex formation by *Escherichia coli* RNA polymerase. *Proc Natl Acad Sci U S A* 2007;104:7833–7838. [PubMed: 17470797]
24. Kontur WS, Saecker RM, Capp MW, Record MT Jr. Late steps in the formation of *E. coli* RNA polymerase- $\lambda P_R$  promoter open complexes: characterization of conformational changes by rapid [perturbant] upshift experiments. *J Mol Biol* 2008;376:1034–1047. [PubMed: 18191943]
25. Bloomfield, V.; Crothers, DM.; Tinoco, I., Jr., editors. *Nucleic Acids: Structures, Properties, and Functions*. University Science Books; Sausalito, CA: 2000.
26. Spolar RS, Record MT Jr. Coupling of local folding to site-specific binding of proteins to DNA. *Science* 1994;263:777–784. [PubMed: 8303294]
27. Kontur WS, Saecker RM, Davis CA, Capp MW, Record MT Jr. Solute probes of conformational changes in open complex ( $RP_o$ ) formation by *Escherichia coli* RNA polymerase at the  $\lambda P_R$  promoter: evidence for unmasking of the active site in the isomerization step and for large-scale coupled folding in the subsequent conversion to  $RP_o$ . *Biochemistry* 2006;45:2161–2177. [PubMed: 16475805]



28. Burgess RR, Jendrisak JJ. A procedure for the rapid, large-scale purification of Escherichia coli DNA-dependent RNA polymerase involving Polymin P precipitation and DNA-cellulose chromatography. *Biochemistry* 1975;14:4634–4638. [PubMed: 1101952]
29. Craig ML, Suh WC, Record MT Jr. HO and DNase I probing of E  $\sigma^{70}$  RNA polymerase- $\lambda$ P<sub>R</sub> promoter open complexes: Mg<sup>2+</sup> binding and its structural consequences at the transcription start site. *Biochemistry* 1995;34:15624–15632. [PubMed: 7495790]
30. Leirmo, S. The Mechanism of Interaction of E. coli RNA Polymerase with Bacteriophage and Bacterial Promoters. Department of Biochemistry, University of Wisconsin-Madison; Madison: 1989.
31. Glaser BT, Bergendahl V, Anthony LC, Olson B, Burgess RR. Studying the salt dependence of the binding of  $\sigma^{70}$  and  $\sigma^{32}$  to core RNA polymerase using luminescence resonance energy transfer. *PLoS One* 2009;4:e6490. [PubMed: 19649256]
32. Vander Meulen KA, Saecker RM, Record MT Jr. Formation of a wrapped DNA-protein interface: experimental characterization and analysis of the large contributions of ions and water to the thermodynamics of binding IHF to H' DNA. *J Mol Biol* 2008;377:9–27. [PubMed: 18237740]
33. Davis CA, Capp MW, Record MT Jr. Saecker RM. The effects of upstream DNA on open complex formation by Escherichia coli RNA polymerase. *Proc Natl Acad Sci U S A* 2005;102:285–290. [PubMed: 15626761]
34. Murakami KS, Masuda S, Campbell EA, Muzzin O, Darst SA. Structural basis of transcription initiation: an RNA polymerase holoenzyme-DNA complex. *Science* 2002;296:1285–1290. [PubMed: 12016307]
35. Vassilyev DG, Sekine S, Laptenko O, Lee J, Vassilyeva MN, Borukhov S, Yokoyama S. Crystal structure of a bacterial RNA polymerase holoenzyme at 2.6 Å resolution. *Nature* 2002;417:712–719. [PubMed: 12000971]
36. Murakami KS, Darst SA. Bacterial RNA polymerases: the whole story. *Curr Opin Struct Biol* 2003;13:31–39. [PubMed: 12581657]
37. Lane WJ, Darst SA. Molecular evolution of multisubunit RNA polymerases: structural analysis. *J Mol Biol* 2010;395:686–704. [PubMed: 19895816]
38. Schroeder LA, Gries TJ, Saecker RM, Record MT Jr. Harris ME, DeHaseth PL. Evidence for a tyrosine-adenine stacking interaction and for a short-lived open intermediate subsequent to initial binding of Escherichia coli RNA polymerase to promoter DNA. *J Mol Biol* 2009;385:339–349. [PubMed: 18976666]
39. Tomsic M, Tsujikawa L, Panaghie G, Wang Y, Azok J, deHaseth PL. Different roles for basic and aromatic amino acids in conserved region 2 of Escherichia coli  $\sigma^{70}$  in the nucleation and maintenance of the single-stranded DNA bubble in open RNA polymerase-promoter complexes. *J Biol Chem* 2001;276:31891–31896. [PubMed: 11443133]
40. Schroeder LA, Karpen ME, deHaseth PL. Threonine 429 of Escherichia coli  $\sigma^{70}$  is a key participant in promoter DNA melting by RNA polymerase. *J Mol Biol* 2008;376:153–165. [PubMed: 18155246]
41. Helmann JD, deHaseth PL. Protein-nucleic acid interactions during open complex formation investigated by systematic alteration of the protein and DNA binding partners. *Biochemistry* 1999;38:5959–5967. [PubMed: 10320321]
42. Fenton MS, Lee SJ, Gralla JD. Escherichia coli promoter opening and -10 recognition: mutational analysis of  $\sigma^{70}$ . *Embo J* 2000;19:1130–1137. [PubMed: 10698953]
43. Vassilyev DG, Vassilyeva MN, Perederina A, Tahirov TH, Artsimovitch I. Structural basis for transcription elongation by bacterial RNA polymerase. *Nature* 2007;448:157–162. [PubMed: 17581590]
44. Mekler V, Kortkhonjia E, Mukhopadhyay J, Knight J, Revyakin A, Kapanidis AN, Niu W, Ebright YW, Levy R, Ebright RH. Structural organization of bacterial RNA polymerase holoenzyme and the RNA polymerase-promoter open complex. *Cell* 2002;108:599–614. [PubMed: 11893332]
45. Ederth J, Artsimovitch I, Isaksson LA, Landick R. The downstream DNA jaw of bacterial RNA polymerase facilitates both transcriptional initiation and pausing. *J Biol Chem* 2002;277:37456–37463. [PubMed: 12147705]
46. Camara B, Liu M, Reynolds J, Shadrin A, Liu B, Kwok K, Simpson P, Weinzierl R, Severinov K, Cota E, Matthews S, Wigneshweraraj SR. T7 phage protein Gp2 inhibits the Escherichia coli RNA

- polymerase by antagonizing stable DNA strand separation near the transcription start site. *Proc Natl Acad Sci USA* 2010;107:2247–2252. [PubMed: 20133868]
47. Bartlett MS, Gaal T, Ross W, Gourse RL. RNA polymerase mutants that destabilize RNA polymerase-promoter complexes alter NTP-sensing by *rrn* P1 promoters. *J Mol Biol* 1998;279:331–345. [PubMed: 9642041]
48. Lane WJ, Darst SA. Molecular evolution of multisubunit RNA polymerases: sequence analysis. *J Mol Biol* 2010;395:671–685. [PubMed: 19895820]
49. Chlenov M, Masuda S, Murakami KS, Nikiforov V, Darst SA, Mustaev A. Structure and function of lineage-specific sequence insertions in the bacterial RNA polymerase  $\beta'$  subunit. *J Mol Biol* 2005;353:138–154. [PubMed: 16154587]
50. Craig ML, Tsodikov OV, McQuade KL, Schlx PE Jr, Capp MW, Saecker RM, Record MT Jr. DNA footprints of the two kinetically significant intermediates in formation of an RNA polymerase-promoter open complex: evidence that interactions with start site and downstream DNA induce sequential conformational changes in polymerase and DNA. *J Mol Biol* 1998;283:741–756. [PubMed: 9790837]
51. Li XY, McClure WR. Characterization of the closed complex intermediate formed during transcription initiation by *Escherichia coli* RNA polymerase. *J Biol Chem* 1998;273:23549–23557. [PubMed: 9722594]
52. Murakami KS, Masuda S, Darst SA. Structural basis of transcription initiation: RNA polymerase holoenzyme at 4 Å resolution. *Science* 2002;296:1280–1284. [PubMed: 12016306]
53. Benoff B, Yang H, Lawson CL, Parkinson G, Liu J, Blatter E, Ebright YW, Berman HM, Ebright RH. Structural basis of transcription activation: the CAP- $\alpha$ CTD-DNA complex. *Science* 2002;297:1562–1566. [PubMed: 12202833]
54. Holbrook JA, Tsodikov OV, Saecker RM, Record MT Jr. Specific and non-specific interactions of integration host factor with DNA: thermodynamic evidence for disruption of multiple IHF surface salt-bridges coupled to DNA binding. *J Mol Biol* 2001;310:379–401. [PubMed: 11428896]
55. Saecker RM, Record MT Jr. Protein surface salt bridges and paths for DNA wrapping. *Curr Opin Struct Biol* 2002;12:311–319. [PubMed: 12127449]
56. Schwartz EC, Shekhtman A, Dutta K, Pratt MR, Cowburn D, Darst S, Muir TW. A full-length group 1 bacterial sigma factor adopts a compact structure incompatible with DNA binding. *Chem Biol* 2008;15:1091–1103. [PubMed: 18940669]
57. Huo YX, Rosenthal AZ, Gralla JD. General stress response signalling: unwrapping transcription complexes by DNA relaxation via the  $\sigma^{38}$  C-terminal domain. *Mol Microbiol* 2008;70:369–378. [PubMed: 18761624]
58. Rosenthal AZ, Kim Y, Gralla JD. Poising of *Escherichia coli* RNA polymerase and its release from the  $\sigma^{38}$  C-terminal tail for *osmY* transcription. *J Mol Biol* 2008;376:938–949. [PubMed: 18201723]
59. Rosenthal AZ, Hu M, Gralla JD. Osmolyte-induced transcription: –35 region elements and recognition by  $\sigma^{38}$  (*rpoS*). *Mol Microbiol* 2006;59:1052–1061. [PubMed: 16420371]

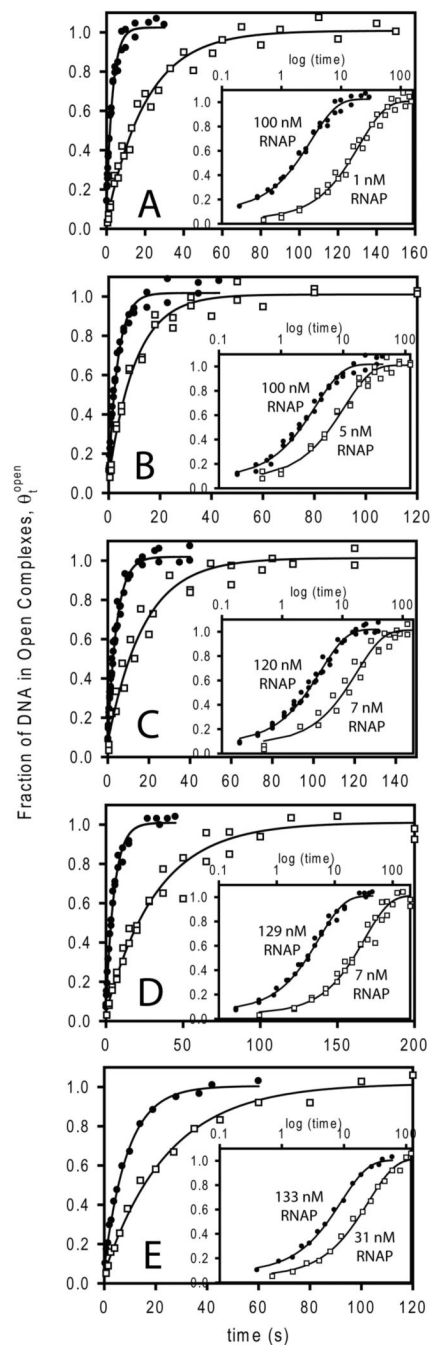


**Figure 1.**

Representative kinetic data for formation of open complexes at the  $\lambda P_R$  promoter at high (closed circles) and low (open squares) concentrations of active RNAP (where RNAP is in excess over promoter DNA) at five different  $[Na^+]$  at 25 °C in NaCl buffer. All data shown here were obtained using rapid quench mixing; the fraction of promoter DNA in the form of open complexes  $\theta_i^{open}$  as a function of time ( $t$ ) was determined using nitrocellulose filter binding after association reactions were quenched with the competitor heparin. Theoretical curves through the data are the best fits to eq 1; corresponding first order irreversible rate constants  $k_{obs}$  for each [RNAP] are given in Supplemental Table 1. Insets replot the data as a function of  $\log t$ ,

demonstrating the single exponential character of the kinetics over the entire time range. (A) 0.15 M Na<sup>+</sup>. (B) 0.17 M Na<sup>+</sup>. (C) 0.19 M Na<sup>+</sup>. (D) 0.21 M Na<sup>+</sup>. (E) 0.23 Na<sup>+</sup>.

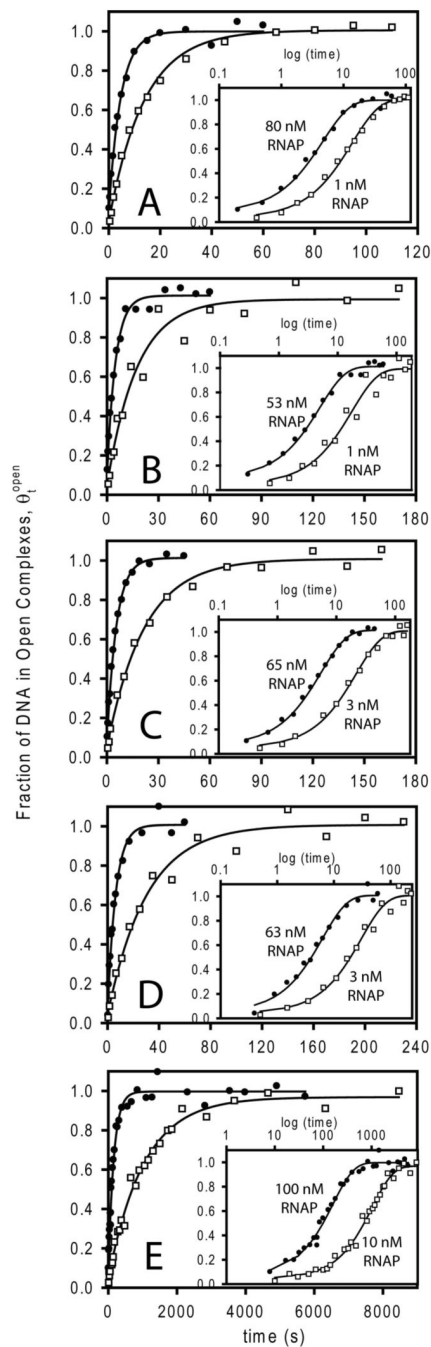


**Figure 2.**

Representative kinetic data for formation of open complexes at the  $\lambda P_R$  promoter at representative high (closed circles) and low (open squares) concentrations of active RNAP at five different  $[Na^+]$  at 25 °C in NaGlu buffer. (Details and insets as in Fig 1; values of  $k_{obs}$  for each  $[RNAP]$  are given in Supplemental Table 2.) With the exception of (E), all data were obtained using rapid quench mixing. (A) 0.23 M  $Na^+$ . (B) 0.25 M  $Na^+$ . (C) 0.27 M  $Na^+$ . (D) 0.29 M  $Na^+$ . (E) 0.55 M  $Na^+$ .

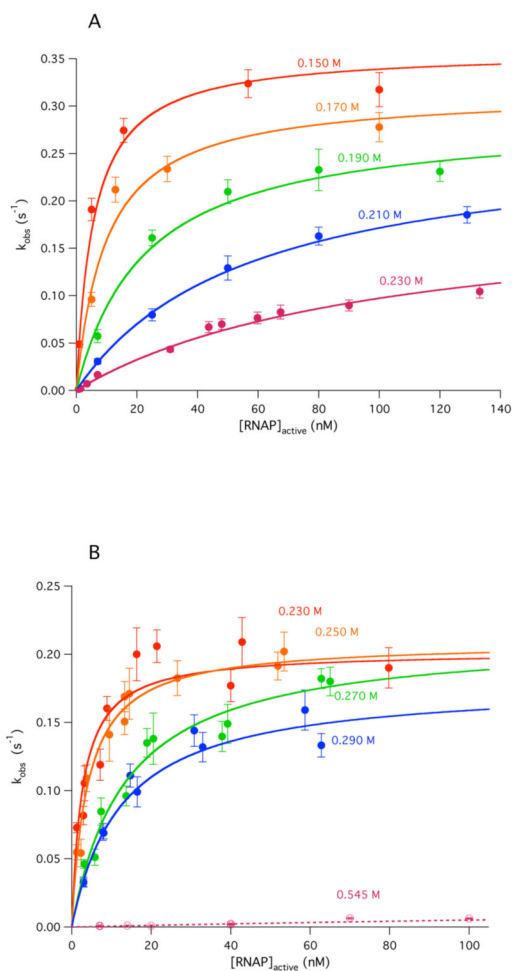


**Figure 3.** Irreversible forward rate constant  $k_{\text{obs}}$  plotted as a function of the total, active RNAP concentration at five different [Na<sup>+</sup>] in Cl<sup>-</sup> buffer (cf. Fig 1) (A) and in Glu<sup>-</sup> buffer (cf. Fig 2) (B). With the exception of data obtained by manual mixing at 0.55 M Na<sup>+</sup> in Glu<sup>-</sup>, data were obtained by rapid mixing and nonlinearly fit to eq 2, yielding values of  $K_1$ ,  $k_2$  and  $k_a$  (see Table 1) for each [Na<sup>+</sup>] investigated.

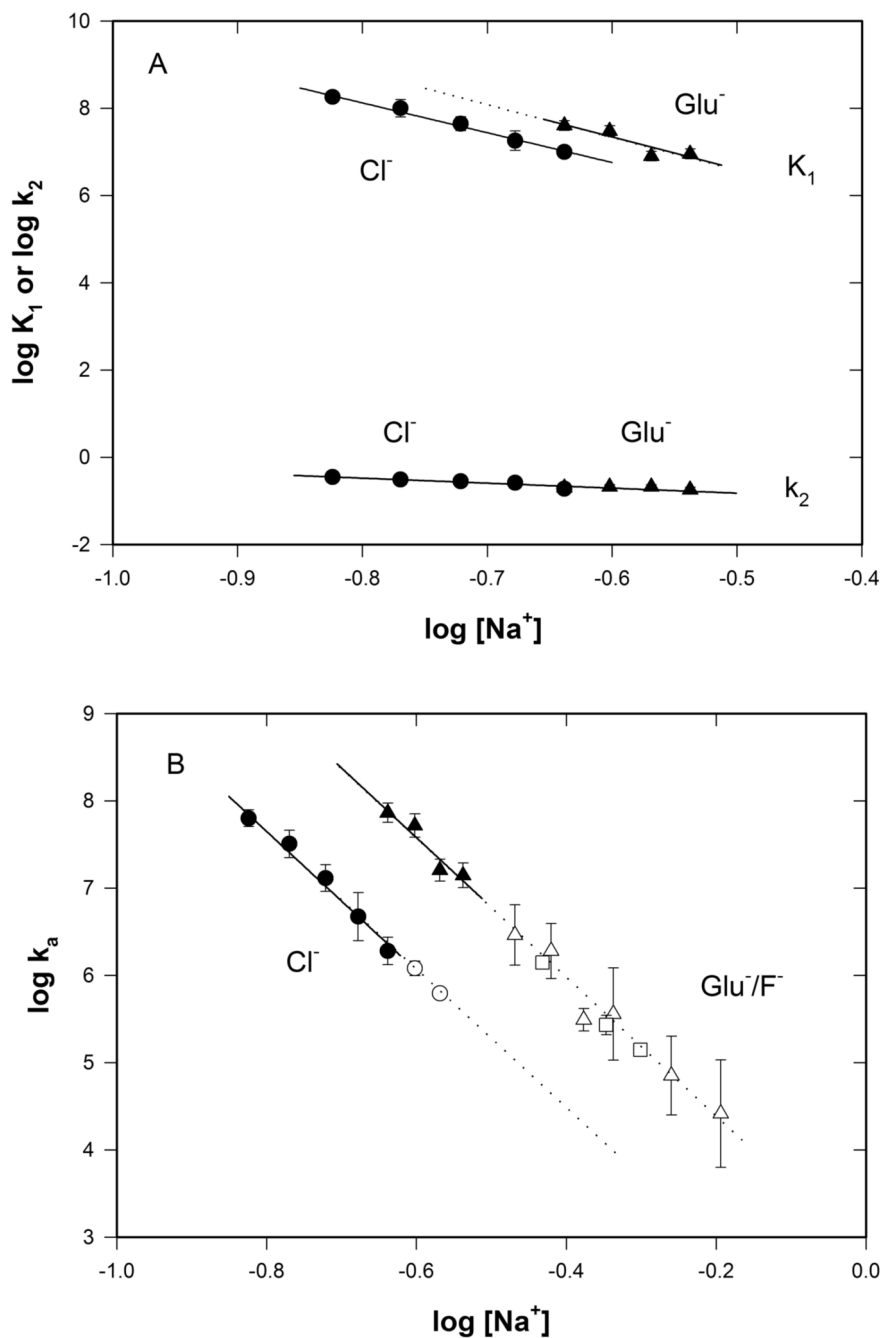


**Figure 4.**

Log-log  $[\text{Na}^+]$ -dependence of  $K_1$ ,  $k_2$  and  $k_a$  as a function of anion. (A) Data from rapid mixing experiments (cf. Fig 3) fit to eq 2 allow a dissection of  $k_a (=K_1k_2)$  into individual values of  $K_1$  and  $k_2$  in NaCl (circle) and NaGlu (triangle) buffers. (B) Values of  $\log k_a$  as a function of  $\log [\text{Na}^+]$  in NaCl (circle), NaGlu (triangle), and NaF (square) buffers. Closed and open symbols represent values of  $k_a$  obtained using rapid and manual mixing, respectively. Dashed lines represent linear extrapolations of the log-log fits to the individual data sets, drawn for purposes of comparing the slopes for the different anions. Values of the log-log slopes  $Sk_a$ ,  $SK_1$  and  $Sk_2$  are given in Table 1 (see Methods for details of the fitting).

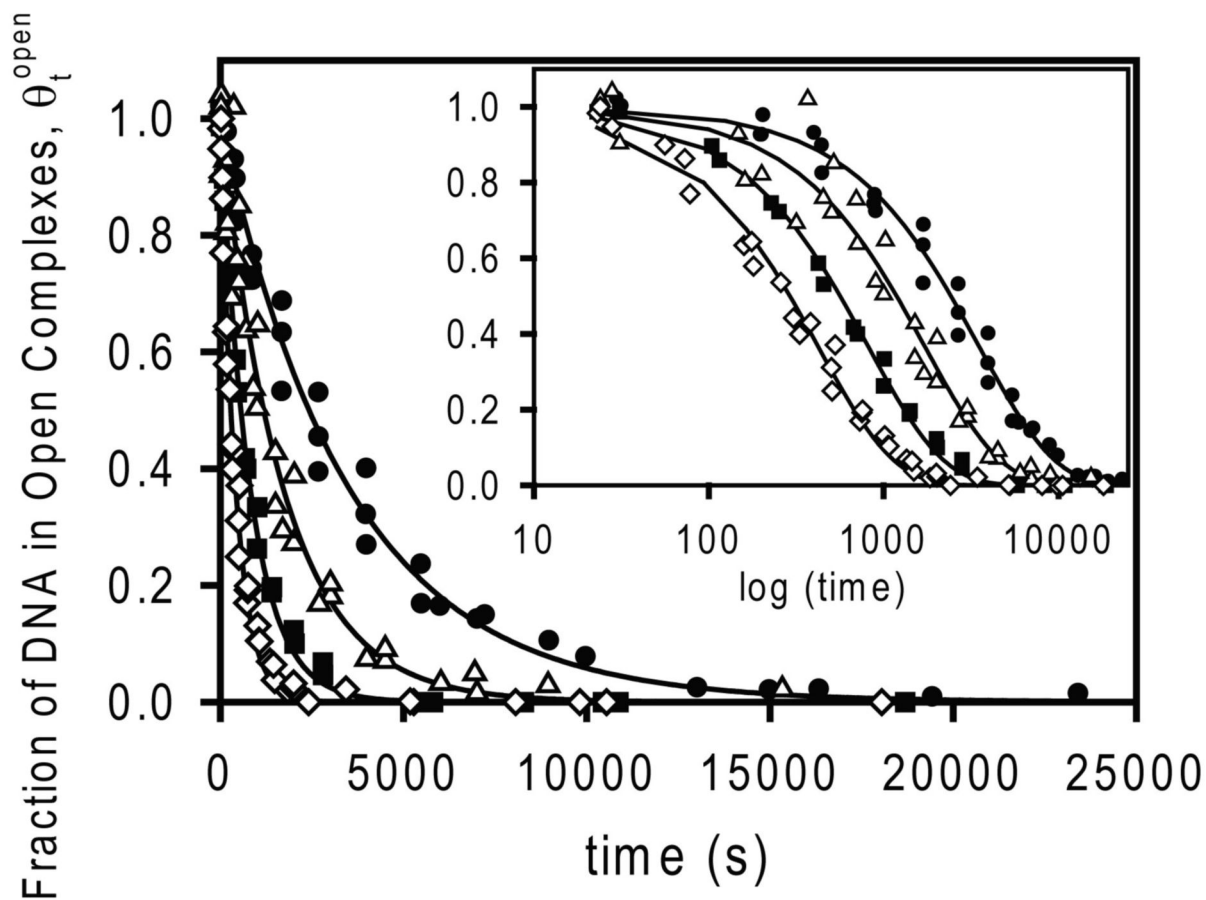


**Figure 5.**

Kinetics of the irreversible dissociation of open complexes at the  $\lambda P_R$  promoter in NaCl buffer at 25 °C. Representative values of  $\theta_t^{open}$  as a function of time (t) determined using nitrocellulose filter binding at four different  $[Na^+]$ : 0.23 M (filled circles), 0.25 M (open triangles), 0.27 M (filled squares) and 0.29 M  $Na^+$  (open diamonds). Theoretical curves through the data are the best fits to eq 4; corresponding first order dissociation rate constants  $k_d$  for each  $[RNAP]$  are given in Table 2. Insets replot  $\theta_t^{open}$  as a function of  $\log t$ , demonstrating the single exponential character of the kinetics over the entire time range.



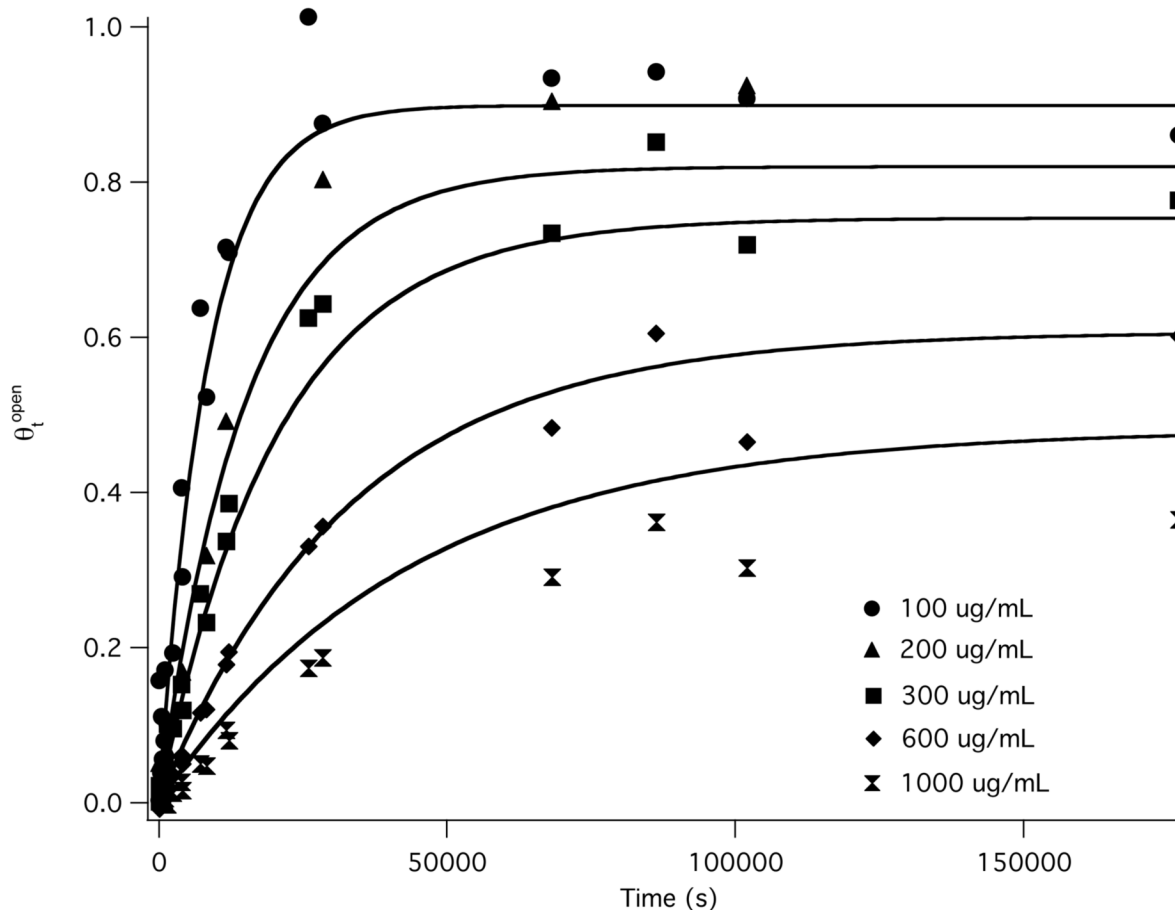


**Figure 6.**

Decay to equilibrium kinetics of promoter association-dissociation at high glutamate (25 °C, 0.46 M  $\text{Glu}^-$ ) and low, constant RNAP concentrations buffered by heparin. The fraction of promoter DNA in open complexes  $\theta_t^{open}$  is plotted as a function of  $\log t$ , where  $t$  is the time after addition of promoter DNA (12.5 pM final) to a solution of RNAP (10 nM total concentration) and heparin at total concentrations of 100  $\mu\text{g/mL}$ , 200  $\mu\text{g/mL}$ , 300  $\mu\text{g/mL}$ , 600  $\mu\text{g/mL}$  and 1000  $\mu\text{g/mL}$ . Data points are from two independent experiments at each heparin concentration are plotted, except for 200  $\mu\text{g/mL}$  which was done once. Fits shown are to the single-exponential decay to equilibrium kinetic equations derived for this situation (eqs 5-6 in Methods). From the observed first order rate constant, analyzed using the best fit value of the association rate constant  $k_a$  for these conditions (Fig 4B), the dissociation rate constant  $k_d$ , the free RNA polymerase concentration, and the equilibrium binding constant  $K_{\text{heparin}}$  for binding RNAP to heparin are determined (see Table 3 and supplemental Table 3).

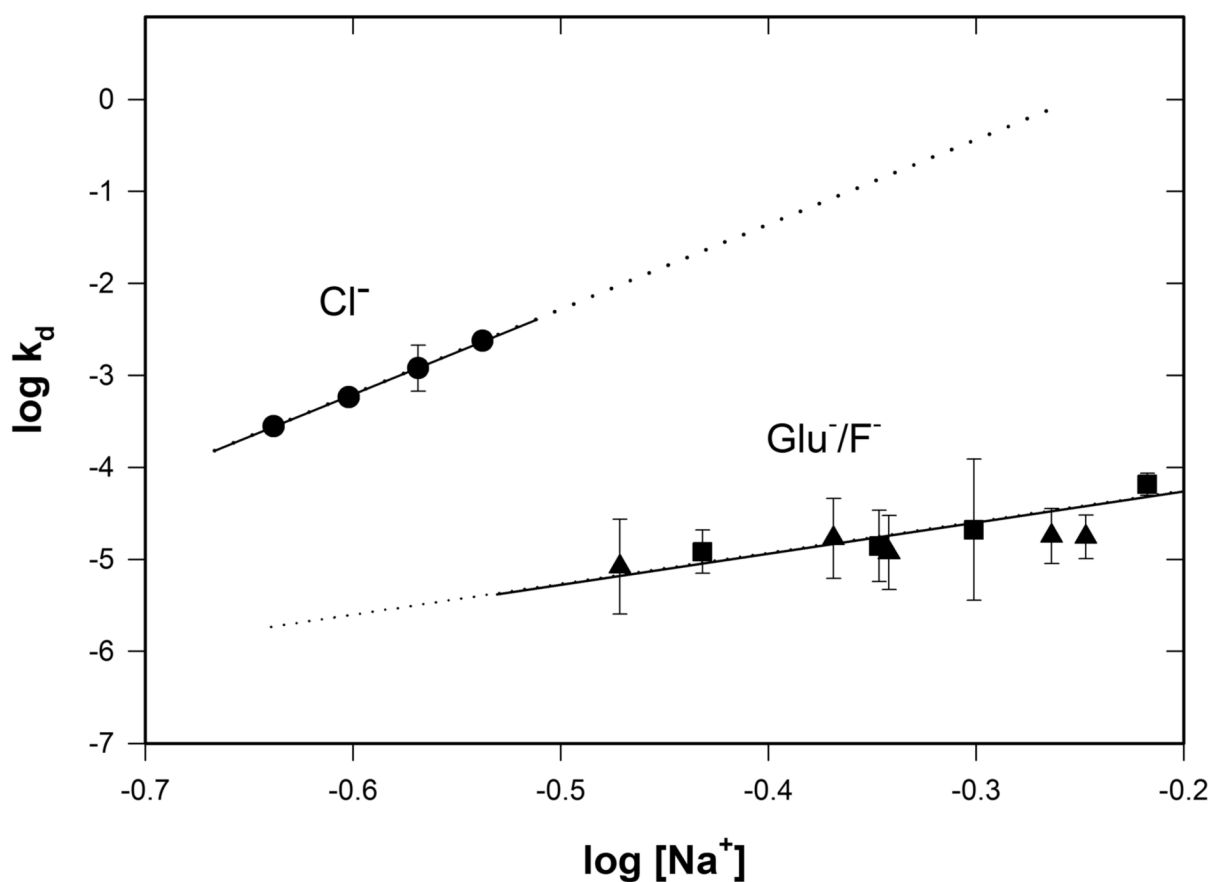


**Figure 7.**

Log-log plot of dissociation rate constants  $k_d$  of RNAP- $\lambda\sigma_R$  promoter open complexes as a function of  $[Na^+]$  in  $Cl^-$  and in  $Glu^-$  or  $F^-$  buffers at 25 °C. Values of  $k_d$  in  $Cl^-$  are from irreversible dissociation experiments of Fig 5; values of  $k_d$  in  $Glu^-$  and  $F^-$  are from reversible dissociation experiments like those in Fig 6. Values of  $k_d$  are reported in Table 2.

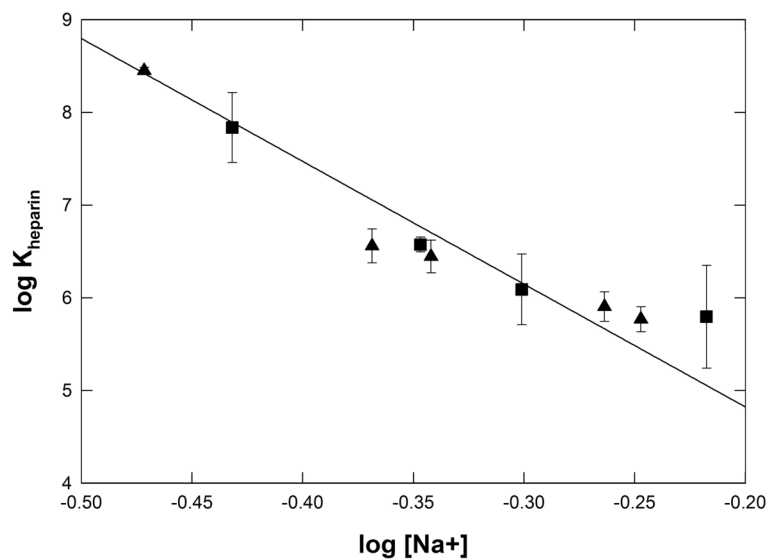


**Figure 8.** Log-log plot of the heparin binding constant  $K_{\text{heparin}}$  as a function of  $[\text{Na}^+]$  for experiments in  $\text{Glu}^-$  and  $\text{F}^-$  buffers at 25 °C. A linear fit of these data yields  $S K_{\text{heparin}} = (\text{dlog} K_{\text{heparin}} / \text{dlog} [\text{Na}^+]) = -13.2 \pm 0.8$  and an extrapolated 1 M  $\text{Na}^+$  intercept of  $2.2 \pm 0.3$ .

### Open Complex Formation: Proposals for Large-Scale Conformational Changes

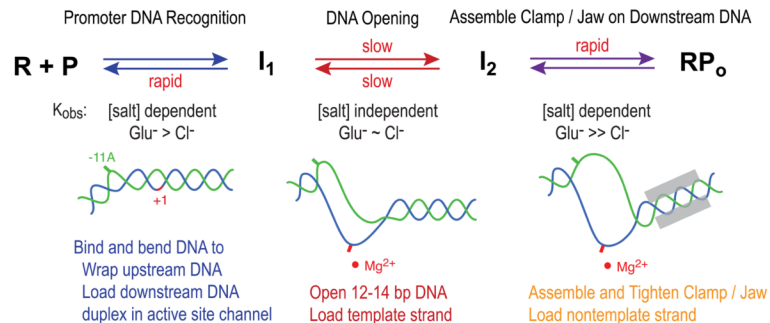


**Figure 9.** Overview of the steps of  $RP_o$  formation, proposed conformational changes and the effects of [salt] and anion on each. Schematic based on results in (23,24,27,33, Gries et al., unpublished).

Table 1

Values of  $k_a$ ,  $K_1$  and  $k_2$  as a function of  $\text{Na}^+$  and anion ( $\text{Cl}^-$ ,  $\text{Glu}^-$  or  $\text{F}^-$ ) for  $\text{RP}_0$  formation at the  $\lambda\text{PR}$  promoter at 25 °C<sup>a</sup>

$\text{Na}^+$ (M)	$k_a$ ( $\text{M}^{-1}\text{s}^{-1}$ )			$K_1$ ( $\text{M}^{-1}$ )			$k_2$ ( $\text{s}^{-1}$ )		
	$\text{Cl}^-$	$\text{Glu}^-$	$\text{F}^-$	$\text{Cl}^-$	$\text{Glu}^-$	$\text{Glu}^-$	$\text{Cl}^-$	$\text{Cl}^-$	$\text{Glu}^-$
A	0.15	$(6.3 \pm 0.6) \times 10^7$		$(1.8 \pm 0.2) \times 10^8$			$(3.5 \pm 0.1) \times 10^{-1}$		
	0.17	$(3.2 \pm 0.5) \times 10^7$		$(1.0 \pm 0.2) \times 10^8$			$(3.1 \pm 0.1) \times 10^{-1}$		
	0.19	$(1.3 \pm 0.2) \times 10^7$		$(4.4 \pm 0.7) \times 10^7$			$(2.8 \pm 0.2) \times 10^{-1}$		
	0.21	$(4.7 \pm 1.3) \times 10^6$		$(1.8 \pm 0.4) \times 10^7$			$(2.6 \pm 0.3) \times 10^{-1}$		
	0.23	$(1.9 \pm 0.3) \times 10^6$		$(7.3 \pm 0.8) \times 10^7$			$(1.9 \pm 0.2) \times 10^{-1}$		$(2.0 \pm 0.1) \times 10^{-1}$
	0.25			$(5.2 \pm 0.7) \times 10^7$			$(2.5 \pm 0.3) \times 10^8$		$(2.1 \pm 0.1) \times 10^{-1}$
	0.27			$(1.6 \pm 0.2) \times 10^7$			$(7.3 \pm 0.8) \times 10^7$		$(2.1 \pm 0.1) \times 10^{-1}$
	0.29			$(1.4 \pm 0.2) \times 10^7$			$(8.0 \pm 0.9) \times 10^7$		$(1.8 \pm 0.1) \times 10^{-1}$
$\text{SK}^b$	$-8.0 \pm 0.6$	$-8.0 \pm 1.7$		$-6.8 \pm 0.3$	$-7.5 \pm 2.3$		$-1.1 \pm 0.2$		$-0.9 \pm 0.3$
B	0.25	$(1.2 \pm 0.1) \times 10^6$							
	0.27	$(6.2 \pm 0.3) \times 10^5$							
	0.34								
	0.37	$(2.9 \pm 1.0) \times 10^6$				$(1.4 \pm 0.1) \times 10^6$			
	0.38								
	0.42	$(1.9 \pm 0.6) \times 10^6$							
	0.44	$(3.1 \pm 0.4) \times 10^5$							
	0.45					$(2.7 \pm 0.3) \times 10^5$			
	0.46	$(3.6 \pm 1.9) \times 10^5$							
	0.50					$(1.4 \pm 0.1) \times 10^5$			
	0.55	$(7.1 \pm 3.2) \times 10^4$							
	0.64	$(2.6 \pm 1.6) \times 10^4$							
$\text{SK}^c$	$-8.0 \pm 0.2$								$-8.3 \pm 0.2$

<sup>a</sup>For 0.15-0.23 M  $\text{Na}^+$  in NaCl buffer and 0.23-0.29 M  $\text{Na}^+$  in NaGlu buffer (part A of the table), values of  $k_a$ ,  $K_1$  and  $k_2$  determined from fits of rapid quench mixing data to eq 2. For 0.34 – 0.64 M  $\text{Na}^+$  (part B of the table), the value of  $k_a$  was determined from fits of manual mixing data to eq 3; values of  $k_{\text{obs}}$  as a function of [RNAP] in this [salt] range do not determine  $K_1$  and  $k_2$  (see text).

<sup>b</sup>SK =  $-\text{dlog}X/\text{dlog}[\text{Na}^+]$  where X =  $k_2$ , K1 or  $k_2$ ; each SK value determined from fits of the data in section A of the table.

<sup>c</sup>Values of SK determined from fitting data from section A and B.

**Table 2**

Values of  $k_d$  as a function of  $\text{Na}^+$  and anion ( $\text{Cl}^-$ ,  $\text{Glu}^-$  or  $\text{F}^-$ ) for the dissociation of  $\text{RP}_O$  at the  $\lambda\text{P}_R$  promoter at 25 °C

$\text{Na}^+$ (M)	$k_d$ ( $\text{s}^{-1}$ )		
	$\text{Cl}^-$	$\text{Glu}^-$	$\text{F}^-$
0.23	$(2.8 \pm 0.1) \times 10^{-4}$		
0.25	$(5.8 \pm 0.4) \times 10^{-4}$		
0.27	$(1.2 \pm 0.3) \times 10^{-3}$		
0.29	$(2.37 \pm 0.09) \times 10^{-3}$		
0.34		$(8 \pm 4) \times 10^{-6}$	
0.37			$(1.2 \pm 0.3) \times 10^{-5}$
0.43		$(1.7 \pm 0.7) \times 10^{-6}$	
0.45			$(1.4 \pm 0.5) \times 10^{-5}$
0.46		$(1.2 \pm 0.5) \times 10^{-5}$	
0.50			$(2.1 \pm 0.2) \times 10^{-5}$
0.55		$(1.8 \pm 0.5) \times 10^{-5}$	
0.57		$(1.8 \pm 0.4) \times 10^{-5}$	
0.61			$(6.5 \pm 0.8) \times 10^{-5}$
$\text{Sk}_d$	$9.2 \pm 0.1$	$3.2 \pm 0.8$	

Values of  $k_d$  in  $\text{Cl}^-$  buffer determined by direct measure of the irreversible rate of dissociation of  $\text{RP}_O$  initiated by the addition of heparin. Values of  $k_d$  in  $\text{Glu}^-$  and  $\text{F}^-$  buffer determined using a decay to equilibrium experiment (eqs 5-6, see Methods) at 25 °C.  $\text{Sk}_d \equiv (\partial \log k_d / \partial \log [\text{Na}^+])$ . Values of  $k_d$  in  $\text{Glu}^-$  do not differ from those in  $\text{F}^-$  outside of experimental uncertainty and were fit together to determine  $\text{Sk}_d$ .